The Flinders University of South Australia

ELECTRONIC STRUCTURE OF MATERIALS CENTRE

Orbital Momentum Profiles and Binding Energy Spectra for the Complete Valence Shell of Molecular Fluorine

Submitted to Chem. Phys. January 1996

Y. Zheng, C.E. Brion, M.J. Brunger, K. Zhao, A.M. Grisogono, S. Braidwood, E. Weigold, S.J. Chakravorty, E.R. Davidson, A. Sgamellotti and W. von Niessen

ESM-121 January 1996

EMS

Orbital Momentum Profiles and Binding Energy Spectra for the Complete Valence Shell of Molecular Fluorine

Y. Zheng, C.E. Brion
Department of Chemistry, The University of British Columbia, Vancouver, B.C., V6T 1Z1, Canada
M.J. Brunger, K. Zhao, A.M. Grisogono*, S. Braidwood*, E. Weigold†
The Electronic Structure of Materials Centre, The Flinders University of South Australia, Adelaide 5001, Australia
S.J. Chakravorty and E.R. Davidson
Department of Chemistry, Indiana University, Bloomington, IN 47405, USA
A. Sgamellotti
Dipartimento di Chimica, Universita di Perugia, Italy
W. von Niessen
Institut für Physikalische Chemie, Technische Universität, Braunschweig, D-3300 Braunschweig, Germany

Abstract

The first electronic structural study of the complete valence shell binding energy spectrum of molecular fluorine, encompassing both the outer and inner valence regions, is reported. These binding energy spectra as well as the individual orbital momentum profiles have been measured using an energy dispersive multichannel electron momentum spectrometer at a total energy of 1500 eV, with an energy resolution of 1.5 eV and a momentum resolution of 0.1 a.u. The measured binding energy spectra in the energy range of 14-60 eV are compared with the results of ADC(4) many-body Green's function and also direct-CI and MRSD-CI calculations. The experimental orbital electron momentum profiles are compared with SCF theoretical profiles calculated using the target Hartree-Fock approximation with a range of basis sets and with Density Functional Theory predictions in the target Kohn-Sham approximation with non-local potentials. The truncated (aug-cc-pv5z) Dunning basis sets were used for the Density Functional Theory calculations which also include some treatment of correlation via the exchange and correlation potentials. Comparisons are also made with the full ion-neutral overlap amplitude calculated with MRSD-CI wavefunctions. Large, saturated basis sets (199-GTO) were employed for both the high level SCF near Hartree-Fock limit and MRSD-CI calculations to investigate the effects of electron correlation and relaxation.

† present address: Institute of Advanced Studies, Research School of Physical Sciences and Engineering, Australian National University, Canberra, Australia, 0200.

* present address: Land, Space and Optoelectronics Division, D.S.T.O., P.O. Box 1500, Salisbury, S.A. 5108. Australia.

1. Introduction

It has been shown that the combination of measurements by electron momentum spectroscopy (EMS) and high level quantum mechanical calculations provides detailed information on the binding energies, electronic structure, momentum profiles and orbital electron density distributions of electrons of atoms and molecules [1–6]. Such studies are also extending our knowledge of momentum space chemistry and permitting investigation of the relation between electron momentum density distributions and chemical bonding, structure, properties and the potential for reactivity [7]. EMS measurements are also facilitating procedures for improving molecular quantum mechanics [6, 8–10], not only at the SCF and CI level, but also for newer computational methods such as Density Functional Theory [11] for small [12, 13] as well as larger [14] molecules.

These capabilities arise because EMS has , to within a very close approximation, the ability to "image" individual atomic and molecular orbitals in the momentum space representation. More exactly EMS measures a quantity proportional to the spherically averaged square of the ion-neutral overlap for an ionization process. The momentum space and the more familiar position space representation are related through a Fourier transformation of their respective wavefunctions. In particular, EMS measurements of the momentum profiles have been shown to provide a sensitive test of the accuracy of SCF and highly correlated molecular wavefunctions [10, 8, 9, 15, 6]. In most cases, very large basis set, energy optimized, wavefunctions have been found to require (spatially) diffuse functions in order to give an accurate prediction of the orbital momentum distributions, particularly at low momenta (corresponding to the chemically sensitive outer spatial regions of the electron distribution). Such wavefunctions developed through interactive collaboration between quantum theory and EMS measurements have been found to be of an essentially "universal" nature in that they are suitable for quite accurate calculations [8, 10] of a wide range of properties, each emphasizing different regions of phase space. For example total energies, dipole (or quadrupole) moments and momentum profiles respectively emphasize small, medium and large r regions.

Since EMS can access the complete valence shell binding energy range, useful direct assessments of the pole strengths predicted by Many-Body Green's Function (MBGF) and Configuration Interaction (CI) calculations can be made. Such comparisons (for example [10, 16–21]) have been particularly informative in the inner valence region where a significant break down of the independent particle (i.e., orbital) approximation occurs and spectra exhibit complex structure in which the ionization strength is severely split into numerous many-body poles.

Satellite intensities can also be studied by photoelectron spectroscopy (PES) and recently Desjardins et al [22] have compared high resolution synchrotron radiation PES measurements of the complete valence shell spectrum of C_2H_4 with high level CI calculations.

In the course of modern science new chemical knowledge and perspectives have repeatedly been obtained by making comparative studies of elements and compounds in which constituent atoms are systematically varied either down a particular group or across a given row of the periodic table. The wide range of EMS and high level quantum mechanical studies increasingly becoming available [4, 6, 23, 24] affords such possibilities. For example, high level theoretical and experimental studies of several Row 2 (CH_4 [25], NH_3 [15], H_2O [5, 10], and HF [26, 27]) and Row 3 (SiH_4 [28], PH_3 [29], H_2S [30], and HCl [18]) hydrides have been compared [6] incorporating the accurate estimates of the momentum resolution [31] into the calculations. In addition results for the Rows 4 and 5 hydrogen halides (i.e., HBr and HI) have also been reported earlier and compared with HCl and HF [19]. Some years ago EMS measurements and calculations for the diatomic halogens Cl_2 [20], Br_2 [21], and I_2 [32] were carried out.

It has been found that the valence orbital momentum distributions of the heavier hydrogen halides HCl [33, 18], HBr [19] and HI [19], and also those of Cl_2 [20], Br_2 [21], and I_2 [32], are quite well described using reasonable quality SCF wavefunctions. However, in contrast, the shape of the valence orbital momentum profiles of the Row 2 hydrides NH_3, H_2O and HF are only adequately predicted if electron correlation effects are included using MRSD-CI calculations [5, 6, 10, 15, 26] or density functional theory [34]. In view of this situation for the hydrides of N, O, and F, it is of interest to investigate the corresponding homonuclear diatomic molecules O_2, N_2, and F_2 using EMS measurements and associated quantum mechanical calculations. In fact EMS studies of N_2 [35] and O_2 [36, 37] have shown that high quality SCF wavefunctions already provide reasonably adequate prediction of the shape of valence orbital momentum distributions and that electron correlation and relaxation effects on the momentum profiles are small. However prior to the present work no such studies have been reported for F_2.

The F_2 molecule is a system of particular interest since, historically, it has posed particular theoretical problems. For example, at the Hartree-Fock level of approximation, two fluorine atoms are lower in energy than a diatomic fluorine molecule, i.e., it is unbound [38]. As well, using Koopmans' theorem, the Hartree-Fock calculation predicts the order of the vertical ionization potentials to be $1\pi_g < 3\sigma_g < 1\pi_u$, in contrast with those, found by PES experiments [39], which give $1\pi_g < 1\pi_u < 3\sigma_g$. The correct order is obtained by including correlation effects which have a particularly large influence on the ionization energies of the

$1\pi_u$ and $1\pi_g$ orbitals [40]. The doubly excited configuration, with the two electrons from $3\sigma_g$ occupying the $3\sigma_u$ orbital, has been found to make a large contribution to the configuration interaction (CI) wavefunction of the ground state.

From a chemical standpoint fluorine is the most powerful oxidizing agent known and this high reactivity poses particular challenges to the experimentalist not only in sample handling and introduction but also because of interactions with sensitive spectrometer components such as microchannel plate detectors, the sample handling system, and the oil in vacuum pumps. These difficulties have presented formidable challenges in the present work and made the study of F_2 much more difficult than those for the other diatomic halogens [20, 21, 32].

With these various perspectives in mind we now report the first EMS measurements of the complete valence shell binding energy spectra and momentum distributions of F_2. The binding energy spectra are compared with those predicted using a range of many-body treatments. The momentum profile measurements are compared with calculations employing a variety of basis sets up to effectively the Hartree-Fock limit and also correlated CI wavefunctions. Comparison is further made with density functional theory predictions. Following the earlier publications for Cl_2, Br_2, and I_2 [20, 21, 32], the present experimental and theoretical study of F_2 completes the systematic investigation of the diatomic halogen series using electron momentum spectroscopy.

2. Theoretical and Experimental methods

The theory and method of electron momentum spectroscopy have been reviewed extensively in the literature [1–3, 5]. Briefly, an EMS experiment involves high energy electron impact ionization of the target species and coincident detection of the scattered and ejected electrons under predefined scattering kinematics. In symmetric non-coplanar kinematics and the plane wave impulse approximation (PWIA), and within the Born-Oppenheimer approximation, the EMS differential cross section for randomly oriented molecules is given by [1, 3]

$$\sigma_{EMS} = C f_{ee} \int d\hat{\mathbf{p}} |(\bar{p}\Psi_f^{N-1}|\Psi_i^N)|^2 \qquad (1)$$

where the spherical average over momentum space is due to the sum over initial rotational states, and the average over initial vibrational states is approximated by evaluating the overlap integral at the equilibrium nuclear distances [1, 3]. The quantity C, which is a kinematic factor, and f_{ee}, which is the antisymmetrized electron-electron collision (Mott) cross section, have been shown to be effectively constant within the range of relative azimuthal angles ϕ used

under typical symmetric non-coplanar kinematic conditions [1]. $|\Psi_f^{N-1}\rangle$ and $|\Psi_i^N\rangle$ are the final ion and initial molecule many-body wavefunctions. Thus the calculated EMS cross section is essentially proportional to the spherically averaged square of the momentum space overlap (Dyson orbital) between the initial target and final ion states. In many systems, where ground state correlation effects are quite small, the target can be described reasonably accurately by the Hartree-Fock approximation (THFA). In the THFA, the expression for the EMS cross section then reduces to [1, 3]

$$\sigma_{EMS} = Cf_{ee}n_jS_j^f \int d\hat{\mathbf{p}}|\phi_j(\vec{p})|^2 = Cf_{ee}n_jS_j^f F(p), \tag{2}$$

where n_j is the occupancy of orbital j and the spectroscopic factor or pole strength S_j^f is the probability that the ion state consists of a hole in an initial state molecular orbital $\phi_j(\vec{p})$. If final state correlation effects are also negligible, the ion wavefunction contains only a single hole configuration and the spectroscopic factor is unity. When final state correlation is important, the spectroscopic factors for ionization from a given orbital to final states of the same symmetry manifold satisfy the sum rule

$$\sum_j S_j^f = 1. \tag{3}$$

The momentum distribution F(p) is the spherical average of the square of the momentum-space representation of a single-particle orbital belonging to the symmetry manifold. The momentum-space orbital wavefunction $\phi_j(\vec{p})$ is related to the position-space counterpart $\psi_j(\vec{r})$ by the Fourier transform.

Recently, eq. (1) has been re-interpreted in the context of Kohn-Sham density functional theory by Duffy *et al* [11]. In particular, Duffy *et al* [11] and Casida [41] have shown that the solutions to the Kohn-Sham equation are, to the first approximation, Dyson orbitals for the primary hole states. Hence in the Target Kohn-Sham approximation (TKSA) eq. (1) becomes

$$\sigma_{EMS} = Cf_{ee}n_j \int d\hat{\mathbf{p}} \mid \phi_j^{KS}(\vec{p}) \mid^2 \tag{4}$$

It is noteworthy that the TKSA formulation of the EMS cross-section provides for inclusion of electron correlation and exchange effects in the target ground state through the exchange-correlation potential and this can be important in the calculation of momentum profiles for some targets [11, 14]. It should also be noted that no binding energy satellites are predicted in this approximation. The results of such TKSA density functional theory calculations have

recently been compared with near Hartree-Fock limit and MRSD-CI overlap calculations and EMS measurements for the valence orbital momentum profiles of acetone [13] and ethylene [12].

The present measurements were obtained using the symmetric non-coplanar instrumentation located at the Flinders University of South Australia. This energy-dispersive multichannel EMS spectrometer [42, 43] has two hemispherical analysers that are used for selecting energetically the scattered and ejected electrons respectively in the experiment. The mean polar angles θ of the two hemispherical analysers are fixed at $\theta = 45°$. The relative azimuthal angle ϕ between the two analyser systems can be varied over a range of $\pm 30°$ under computer control. In the present experiment the energy of the incident electron beam was 1500 eV plus the binding energy and the energy range sampled by each analyser with the microchannel plate position sensitive detectors is set at 750 ± 7.5 eV. The overall energy resolution of the spectrometer due to the energy spread of the incident electron beam and the two hemispherical analysers was measured to be 1.5 eV FWHM using the helium 1s binding energy spectrum. The momentum resolution is estimated to be 0.1 a.u. FWHM. Details of the instrument and data handling procedures can be found elsewhere [3, 42, 43].

Molecular fluorine gas was introduced into the interaction region via a specially constructed stainless steel reservoir and inlet system with a Granville-Phillips leak valve. The extremely high reactivity of F_2 required careful sample handling and disposal. Fluorine gas was obtained from Melbourne University (Dr. T. O'Donnell) in a relatively low pressure (3 atm) stainless steel chamber to avoid the use of a gas regulator. The gas was expanded into a stainless steel storage reservoir and inlet system which was purged several times to remove the oxidized and desorbed species from the walls. The purging fluorine gas and products were allowed to react with anhydrous alumina ($2Al_2O_3 + 6F_2 \rightarrow 4AlF_3 + 3O_2$) placed in a chamber situated between the storage reservoir and the isolated sample pumping system. This procedure was essential not only to obtain a high purity F_2 sample in the reservoir but also for the prevention of damage to the rotary pump and oil from highly exothermic oxidation by F_2 when evacuating the sample system. When all reaction with F_2 was completed the chamber could be evacuated safely. Serious deterioration of the microchannel plate (MCP) detectors in the EMS spectrometer was experienced while studying F_2 and several sets of plates had to be replaced during the measurements. These difficulties are due to the high surface area and low conductance of the MCP microchannel architecture. This situation placed serious limitations on the measuring time and the statistical precision of the data obtained for F_2. Furthermore careful checks had to be made for any changes in the energy scale that occurred due to reaction of F_2 on critical surfaces in the spectrometer. Two independent sets of experiments were performed,

spaced by about three years. While reasonable binding energy spectra were obtained the statistical precision of the momentum profile measurements for F_2 is somewhat inferior to that in previous studies of other molecules.

3.Computational methods for momentum profiles

Spherically averaged theoretical momentum profiles (TMPs) of the valence orbitals of F_2 have been calculated using the THFA (eq.2) with several basis sets, ranging from the minimal basis to the near-Hartree-Fock limit, and also using DFT in the TKSA with the Becke-Perdew density gradient approximation and a large basis set (see below). The effects of electron correlation and relaxation have been investigated by using the multi-reference singles and doubles configuration interaction (MRSD-CI) many-body wavefunctions in the ion-neutral overlap distribution (OVD) using eq.1. The TMPs include allowance for the orbital degeneracies and the momentum resolution is in corporated using the GW-PG method [31]. Thus these TMPs can be compared directly with the experimental momentum profiles (XMPs).

The basis sets and methods used for the SCF, TKSA-DFT and MRSD-CI calculations of the valence electron momentum profiles of F_2 are briefly described below and predicted total energies, quadrupole moment Θ_{zz} values and p_{max} of the $1\pi_g$ momentum profiles of fluorine are listed in Table 1 along with the actual bond length used in each calculation.

(1)*STO-3G:* This is the standard minimal basis set designed by Pople and co workers [44], effectively of single zeta quality, using a single contraction of three Gaussian functions for each basis function. A basis set of [2s1p] is used for each fluorine atom.

(2)*S&B:* This is a Gaussian basis set essentially equivalent in quality to a double zeta basis [45]. A basis set of [4s2p] is used for each fluorine atom.

(3)*6-311+G*:* This is a split valence basis and it comprises an inner shell of six s-type Gaussians, and an outer valence region, which has been split into three parts, represented by three, one and one primitives, respectively. A detailed description of this basis can be found in ref. [46]. Diffuse s- and p-functions (+) are added for the fluorine atoms. In addition, polarization functions (*) are also included in the basis (a single set of five d-type Gaussian functions for the F atom).

(4)*199-GTO:* This extensive Gaussian basis set was developed at Indiana university in the course of the present collaborative work. The primitive basis set for the F atom was constructed starting from the Partridge basis set [47] (18s 13p). One more diffuse s function was added, as prescribed in Ref. [47] for the negative ion. In addition, we extended the basis

set with one more diffuse s function with an exponent of 0.0347 (an even tempered extension). The 13p set was augmented with one more diffuse p function prescribed in Ref. [47] for the negative ion, yielding the 20s 14p set used in this work. The (20s 14p) set was then contracted to a (12s 8p) set. The s functions with the ten largest exponents were contracted into two s-type contractions, using coefficients obtained from the Hartree-Fock 1s and 2s orbitals of the F atom. The ten functions with the smallest exponents were left uncontracted to provide flexibility in representing the numerous positive ion states of F_2 which need accurate description for the present work. The p functions with the seven largest exponents were contracted into one function using coefficients from the 2p orbital from the SCF calculation of the fluorine atom. The 4d, 3f set (pure spherical harmonics) for the F atom used in a previous publication [48] was used to provide polarization as well as some correlation. A g function (pure spherical harmonics) with an exponent of 1.0 was also used to improve the valence shell correlation energy. We have further augmented the basis set with three s, three p, and three d functions at the center of the F_2 bond to form an approximation for the Rydberg orbitals which are populated in the excited ions states of F_2. The exponents for these basis functions were determined to be ($\alpha = 0.027, 0.081, 0.243$).

The results for the SCF and correlation energies are reported in Tables 1 and 2. In Table 3, the SCF orbital energies have been compared with the numerical Hartree Fock values. The agreement between them is satisfactory and thus the basis set can be used for the configuration interaction calculations of the binding energy spectra. In addition to predicting the momentum profiles the present study has also focused on the calculation of the satellite region of the binding energy spectra of the F_2 molecule. Therefore, a reasonably accurate description of excited ions states of the F_2 molecule is needed. These leading Slater determinants for the ion states may be approximated using improved virtual orbitals [49] (IVO) which are made by diagonalizing the Fock operator for the doubly charged ion $^3\Sigma_g^-$ state constructed with the orbitals for the neutral F_2 molecule. Table 3 also lists the orbital energies for the other basis sets used in this paper. Also shown are the virtual orbital energies for the IVOs. These are the binding energies of the Rydberg orbitals of F_2^+ and indicate the adequacy of the basis set in describing excited states of F_2^+.

(5) *199-G(CI):* The occupied Hartree-Fock molecular orbitals and improved virtual orbitals of the ground state of F_2, calculated with the 199-GTO [12s,8p,4d,3f,1g/3s,3p,3d] basis set (see (4) above), were used in the multireference singles and doubles configuration interaction (MRSD-CI) calculations. It may be seen from the experimental spectrum (Fig. 1) that positive ion states have been observed at binding energies as high as 60 eV. Generally, several hundred

positive ion states in each symmetry should be found in order to cover a range of 60 eV. In fact, this range exceeds the second ionization limit of F_2, estimated to be 44 eV (see Table 2), and the number of states found will be limited by the lack of basis functions corresponding to high-n Rydberg states and continuum orbitals. Clearly, the desire to investigate such a large number of states imposes restrictions on the accuracy of the calculation for any one of them. Therefore, these calculations have been simplified by neglecting core-correlation and core-relaxation effects by freezing the 1s core to be the uncorrelated core of the neutral molecule.

The first step in describing this manifold of states was to build an appropriate reference space of Slater determinants suitable for extracting all the desired roots of the positive ion of a particular symmetry. It is obvious that the reference space will not be sufficient for the highly accurate calculation of the correlation energy of any single root, because the correlating configurations and dominant excited state configurations are different for each root. However, it is possible to calibrate the error by calculating the lowest ion state in each symmetry to a very high accuracy.

The MELD package [50] has been used in order to perform the present calculations. All the calculations were performed in the D_{2h} subgroup of the $D_{\infty h}$ point group of the molecule. This causes difficulties in the calculations. Primarily, this increases the size of the CI space. Moreover, it is desirable to keep the CI space closed under the operations from the $D_{\infty h}$ point group. The latter is difficult to impose since it is necessary to use perturbation theory to select the dominant configurations. In order to make the selected CI space invariant, the list of configurations would need to be augmented after perturbation selection was performed, which would make the CI space very large. Instead, the reference space of each CI calculation reported in this work was constructed to be a closed set, therefore ensuring that the dominant part of the calculated wave function and energy obeyed the required symmetry constraints. This proved sufficient for the purposes of this work. The MRSD-CI TMPs were then calculated according to the OVD (Dyson orbital) in eq.1 at the single-root level (199-G(SR-CI)) and multi-root level (199-G(MR-CI)) of approximation. The single-root calculation was carried out for the three outer valence orbitals ($1\pi_g$, $1\pi_u$ and $3\sigma_g$). The multi-root calculation including many roots of each symmetry was performed for the complete valence shell of F_2. It is found that there is no significant difference between the multi-root and single-root momentum profiles for the three outer valence orbitals. The 199-G(MR-CI) treatment has also been used for the MRSD-CI calculation of the complete valence shell binding energy spectrum (see section 4.2 below).

(6)*DFT-PV5Z-BP:* Eq.1 has recently been interpreted in the context of Kohn-Sham density functional theory [11]. In a similar manner to the target Hartree-Fock approximation, eq.1 can be factored in terms of the Kohn-Sham orbitals to give the target Kohn-Sham approximation (TKSA). In this approach exchange and electron correlation in the target ground state are included through Becke's [51] gradient correction to the exchange energy and Perdew's [52] gradient correction to the correlation energy. In the present DFT calculation, the TKSA-DFT orbital momentum profiles were obtained by performing a Fourier transform of the Kohn-Sham orbitals of the neutral fluorine molecule. Kohn-Sham orbitals were calculated [11] using density functional theory with the non-local potentials, i.e. the Becke-Perdew corrections, and a truncated form of the aug-cc-PV5Z basis set. This large basis set, developed by Dunning and co-workers [53], adds both polarization and diffuse functions to an already quintuple-zeta description of the fluorine valence orbitals. In the present calculations the f functions were not included due to limitations of the existing version of the deMon density functional program [54]. It has been checked that this truncation produces negligible change in the shape and magnitude of the calculated momentum profile at the SCF level although the truncation does slightly effect other properties such as the total energy and quadrupole moment. Since the comparison of the property values for the aug-cc-PV5Z calculations in Table 1 (see footnote d) shows that the truncated and the non-truncated versions yield very similar momentum profiles, total energies and Θ_{zz} values to those obtained from the 199-GTO calculation it can be concluded that the Hartree-Fock limit has been closely approached even with the truncation.

4. Results and discussion

Fluorine belongs to the $D_{\infty h}$ point group and the ground state independent particle electron configuration can be written as:

$$(\mathrm{Core})^4 \underbrace{(2\sigma_g)^2(2\sigma_u)^2}_{Inner-valence} \underbrace{(3\sigma_g)^2(1\pi_u)^4(1\pi_g)^4}_{Outer-valence} X^1\Sigma_g^+$$

The ordering of the outer valence orbitals corresponds to that given by the binding energies in PES experiments [39] and CI calculations [40]. Results for the angle resolved binding energy spectra as well as the experimental and theoretical electron momentum profiles for the valence region are conveniently discussed with reference to the above orbital assignments.

4.1 Experimental binding energy spectra

The ionization potentials for the valence electrons of F_2 have been studied previously, although the entire spectrum has not been thoroughly characterized, particularly in the inner valence region. For example, outer valence He I and He II ultraviolet photoelectron spectra (UPS) [55, 56] have given information on the three cation states of F_2 in the binding energy range below 25 eV. X-ray photoelectron spectroscopy (XPS) has been used by Weightman and Thomas [57] to study the inner valence region from 34 to 48 eV. Two prominent broad peaks assigned to ionizations of the $2\sigma_u$ and $2\sigma_g$ orbitals were reported [57] to have binding energies of 37.47±0.05 and 41.75±0.05 eV respectively, while no additional satellite structure peaks were observed over the limited energy range studied.

In the present EMS study, the binding energy spectrum of F_2 was measured over the range from 14 to 60 eV. Fig. 1(a)-(c) show the spectra at $\phi = 10°$ and 0°, and the sum of the spectra at 10° and 0° respectively. The spectra at $\phi = 10°$ and 0° exhibit considerably different relative contributions from the various possible ionization processes. The binding energy spectrum of $\phi = 10°$ ($p \sim 0.8$ a.u.) in Fig. 1(a) illustrates the dominance of "p-type" orbitals, i.e. $1\pi_g$, $1\pi_u$ and $2\sigma_u$, which are anti-symmetric in position space and should go to zero at zero momentum (at perfect momentum resolution). In contrast, the 0° spectrum in Fig.1(b), corresponding to very small momenta ($p \sim 0.1$ a.u.), shows dominant contributions arising from the $3\sigma_g$ and $2\sigma_g$ "s-type" symmetric orbitals. The summed spectrum ($\phi = 0° + 10°$) displays the contributions from both types of processes. Comparison of the $\phi = 0°$ and 10° spectra indicates that there is an accumulation of additional p-type intensity in the 25-35 eV region at $\phi = 10°$. This (see below) is apparently part of the $2\sigma_u$ and/or $1\pi_g$ and $1\pi_u$ inner valence manifolds arising from many-body effects. A prominent broad peak at about 52 eV in the inner valence region above the main $2\sigma_u$ and $2\sigma_g$ peaks is clearly dominantly of s-type and thus can be most likely be assigned to the $2\sigma_g^{-1}$ process. Gaussian deconvolution is used to separate the main transitions due to different ionic states. The Gaussian widths take into account the instrumental width of the EMS spectrometer as well as the respective Franck-Condon widths. The energy positions and Franck-Condon widths of the outer valence ionization peaks are taken from high resolution PES studies [39]. The Franck-Condon widths of the main $2\sigma_u$ and $2\sigma_g$ transitions in the inner valence region were estimated from the spectrum reported by Weightman and Thomas [57]. The fitted Gaussians for each peak are indicated by dashed lines and the corresponding peak positions are marked on the top of Fig. 1(a) while their sums, the overall fitted spectra, are represented by solid lines.

4.2 Calculated binding energy spectra

The complete valence shell binding energy spectrum of F_2 has been calculated in the present work using several theoretical methods employing many-body (electron correlation) treatments. The calculated ionization potentials are shown in comparison with PES [39], XPS [57] and the present EMS measurements in Table 4. The many-body Green's function (MBGF) calculations have been carried out using the ADC(4) method [58] and a [5s4p1d] Gaussian basis set [59]. The direct-CI calculations were performed using the direct-CI method of Saunders and van Lenthe (Mol. Phys. 48 (1993) 933) for the first three ion states of $^2\Sigma_g^+$ and the first four of $^2\Sigma_u^+$ symmetry, with the inclusion in the reference space of all the configurations with coefficients larger than 0.1 and using the Dunning basis set [5s3p1d]. For comparison purposes with the other basis sets and calculations shown in Table 1 it should be noted that the total energies, quadrupole moments and equilibrium internuclear distance are (-198.75327, 0.4915, 1.41193) for the ADC(4) and (-198.75439, 0.6206, 1.435) for the direct-CI calculations respectively. In addition a large MRSD-CI calculation of the binding energy spectrum of F_2 has been carried out using the same 199-G(CI) treatment employed for the theoretical momentum profiles (see sections above and 5 below).

The details of the MRSD-CI binding energy spectrum calculation are as follows. In Table 5, the results for the primary hole states computed as the lowest (single) root in multi-reference CI calculations chosen to give only one correct eigenvalue are reported. All the single root calculations in Table 5 were performed with IVOs. The reference space was determined from smaller CI calculations, and for each symmetry, all configurations with coefficients greater than 0.05 were included in the reference space. In the next step, we have added the missing partners of each reference configuration in order to close the set of configurations under the rotation operators. Perturbation selection was done on all the configurations generated by single and double excitations with a energy threshold of 10^{-7} hartree. In no case did the total estimated energy from the discarded configurations ever exceed 0.16 eV. However, the full CI limit estimated including quadrupole corrections was lower by about 0.04 hartree which is about 1 eV. This is indeed a problem, however, it is observed that the errors in the neutral molecule and the positive ions do tend to cancel out. This leads to an assumption that we have made in this work that the correlation energies obtained from quadrupole excitations from the reference space both in the neutral and positive ion exactly cancel each other. The energies of the peaks labeled, $3\sigma_g$, π_u, π_g are obtained at 21.09, 18.99 and 15.84 eV (see Table 5). These values are all close to the PES experimental measurements (see ref.[39] and Table

4) which yield peaks at 21.10, 18.80 and 15.87 eV.

In Tables 6, 7, 8 and 9, the results of the multi-root CI calculations to determine the energies, S_j^f pole strength values, the dominant configurations and orbital contributions to various excited states in $^2\Sigma_g^+$, $^2\Pi_{xu}$, $^2\Pi_{xg}$, and $^2\Sigma_u^+$ positive ions respectively have been summarized. The reference space for each of the calculations were constructed in stages. First, CI matrices constructed from all the 1p-2h configurations in each symmetry were diagonalized. Only the energy states corresponding to $^2\Sigma_g^+$, $^2\Pi_{xu}$, $^2\Pi_{xg}$, and $^2\Sigma_u^+$ ion states were considered whose energy was less than the approximate second ionization limit (52 eV) found when computing the IVO's. A list of configurations was created from these positive ion states including all coefficients greater than 0.1. In the next step, this list was augmented with the missing configurations in order to close this set under rotations. The next step was to identify all configurations whose diagonal CI matrix element yielded lower energies than any selected root in the reference space and to add these to the reference set. Finally, when no more singly or doubly excited configurations possessing lower energies than any selected root of the reference space was detected, we ended up with a very large reference set which needed to be shortened. In the next stage, this large reference space was diagonalized and the configurations with coefficients above 0.1 in the lowest roots were kept and augmented to be closed under rotations. The energy range spanned by the reference space was approximately 31-35 eV above the lowest root in each symmetry. Increasing the energy range by a few eV would render all these calculations unfeasible considering the disk space and time constraints for each calculation. With this choice of the reference set, each of the perturbation selected MRSDCI calculations were performed.

Prior to the final calculations, the virtual space of orbitals for every CI calculation had to be improved in order to shorten the list of configurations and also optimize the correlation energies of the numerous positive ion states. As noted in the previous work [22], the construction of averaged natural orbitals (ANO) is an useful method. In order to keep the reference set of configurations from being changed, we instead used frozen averaged natural orbitals (FANO) with all orbitals appearing in the reference configurations kept frozen. A relatively smaller CI calculation including about 135000 configurations was performed for the $^2\Sigma_g^+$ states of the F_2 positive ion, and the corresponding average density matrix was formed. For each of the symmetries (Σ_g, Π_g, Π_u, Σ_u) the orbital space not used in the reference configurations was abstracted from this average $^2\Sigma_g^+$ density matrix and diagonalized to yield a set of FANO's for that ion symmetry. Choice of any other symmetry in order to compute the FANO's would cause symmetry breaking within a degenerate pair of orbitals found in two different

symmetries of the D_{2h} subgroup.

It may be seen in Tables 6 through 9 that the size of the CI space for all the CI calculations are several hundred thousands. Due to the unavoidable symmetry breaking caused by the perturbation selection on the closed reference set, the roots were analyzed and identified by computing the overlap with the pure reference set counterparts. It may be seen that only roots of Σ_g, Π_u, Π_g, and Σ_u symmetry are listed because the S_j^f for the other positive ion states would be negligible. This can be verified by considering the coefficients of the dominant configurations of the neutral molecule and their primary hole counterparts. The results for the first CI root reported in Tables 6, 7 and 8 can be compared with the corresponding values in Table 3 in order to estimate the error and thereby the resolution of our CI calculations. The differences between the peak positions are 0.18 (Σ_g), 0.41 (Π_u), and 0.49 eV (Π_g) for the primary peaks between the two CI calculations. Because the 199-G(CI) calculation used a larger basis set designed to describe more of the cation excited states, this calculation gave many more ion states than were found with the stable ground-state neutral molecule basis sets used in the direct-CI and ADC(4) calculations. In particular several states involve the $3d\delta_g$ orbital that is missing in the other basis sets. As seen in Tables 6-9, however, there is little intensity predicted for these extra states. Almost all the states with large pole strength involve a leading configuration with one or more electrons in the $3\sigma_u$ valence anti-bonding orbital. An exception is the $^2\Sigma_g^+$ ion state predicted at 42.77 eV which is dominated by a $(\pi_g)^{-2}(\delta_g)^1$ two-hole one-particle configuration.

4.3 Comparison of calculated and measured binding energy spectra

The measured binding energy spectra for $\phi = 10° + 0°$ are compared in Fig.2 with synthesized theoretical spectra, generated using the energies and pole strengths given by the respective Green's function ADC(4), direct-CI and MRSD-CI calculations in Table 4. In each of these cases the 199-G(CI) wavefunction was used to calculate the angular dependence (i.e. from the momentum profile) at each binding energy using eq. 1. The same overall energy widths, used for the Gaussian fits of the experimental spectra in Fig.1 have been folded into the calculated spectra. The summed experimental spectrum (Fig. 2(a)) is normalized to each theoretical spectrum on the $1\pi_u$ peak.

As noted above the values of calculated ionization potentials (Table 5) in the outer valence region found from the single root MRSD-CI calculation are in quite good accord with experiment at the 199-G(CI) level. From the high resolution PES data from ref. [39] the ionization

potentials of the HOMO ($1\pi_g$), $1\pi_u$, and $3\sigma_g$ orbitals are 15.87, 18.8, and 21.1 eV respectively. The lower resolution EMS IPs are consistent (Table 4) with these high resolution PES data. The lower accuracy multi-root MRSD-CI calculation predicts intense poles for these three transitions at 15.35, 18.58 and 20.91 eV respectively, within 0.3 eV of the experimental values. The ADC(4) calculation (Table 4) gives very similar results for these three orbitals with dominant poles at 15.48, 18.61, and 20.65 eV. The ionization potentials of the two outer valence orbitals were not computed by the direct-CI calculation, which predicted a value of 20.48 eV for the ionization potential for the $3\sigma_g$ orbital. It can also be seen from Fig. 2 that all the calculated spectra have higher intensity than the measured spectra for this orbital. This is consistent with the comparison of the measured and calculated momentum distributions which will be discussed in the next section.

In the inner valence region of 25-60 eV there is obviously significant splitting of the ionization lines due to strong electron correlation effects. All three calculations predict (Table 4) many ion excited states of $^2\Sigma_u^+$ and $^2\Sigma_g^+$ symmetry of appreciable intensity in the energy range of the $2\sigma_u$ and $2\sigma_g$ primary-hole-state configurations. In addition, as shown in Tables 6-9, there are many more states with negligible intensities. Analysis of satellite peaks in the experimental binding energy spectrum is difficult due to the many poles and low resolution of the spectrometer. However, a general comparison of the symmetries and the positions of the experimental and theoretical peaks is informative. For the two main peaks in the inner valence region the ADC(4) calculation is in fair accord with the experimental values for the peak positions of the main energy poles (Table 4). The main energy poles (37.36 and 42.07 eV) given by the direct-CI calculation are also very close to the experimental values of 37.3 and 41.2 eV respectively (see Table 4). The MRSD-CI result predicts the two energies of 37.87 and 42.97 eV for the main poles. All three calculations overestimate the inner valence peak intensities with the normalization (i.e. on the $1\pi_u$ peak) used in Fig. 2 (c). From the comparison of the theoretical and observed momentum distributions in the next section it can also be seen that the 199-G(CI) wavefunction does in fact overestimate the ionization intensity from the two inner orbitals of F_2 (see next section). This discrepancy is probably not due to deficiencies in the wavefunction, but could be due to further energy poles located out of the experimental binding energy range.

The experimental intensity between 25-35 eV appears to be a combination of many poles mostly with a p-type distribution since the intensity is greater at $\phi = 10°$ than at $\phi = 0°$ (compare Fig.1(a) and (b)). Based on orbital symmetry, the intensity must therefore be derived from the $1\pi_g$, $1\pi_u$, or $2\sigma_u$ orbitals. Indeed this is seen in the theoretical prediction as

each of the calculated spectra in Fig. 2 shows contributions from these three orbitals in this energy region. The ADC(4) calculation predicts poles with $1\pi_g$, $1\pi_u$ and $2\sigma_u$ symmetry and the MRSD-CI gives mainly poles with $1\pi_g$ and $2\sigma_u$ symmetry in this energy region. Consideration of the relative intensities of experimental and theoretical momentum profiles suggests that the intensity in the binding energy spectrum between 25 and 30 eV is due primarily to the $1\pi_g$ and/or $2\sigma_u$ inner valence ionization (see next section).

The satellite peak positioned about 52 eV clearly has an s-type distribution (see Fig.1(a) and (b)) and is therefore expected to be associated with $2\sigma_g$ ionization. Both the ADC(4) and MRSD-CI calculations predict fairly large $2\sigma_g$ satellites at 55.6 and 53.11 eV respectively. The direct-CI calculation does not extend into this energy region. The position of the energy pole given by the ADC(4) calculation is about 3.5 eV higher than experiment and the predicted intensity is somewhat larger. On the other hand, the MRSD-CI predicts an energy pole very close to the experimental value, although the intensity is somewhat weaker.

4.4 Experimental and theoretical momentum profiles

Experimental momentum profiles for the outer and inner valence orbitals plus the satellite peaks of F_2 were determined by scanning the azimuthal angle ϕ while measuring in the energy ranges 14-28 eV and 30-50 eV respectively using the energy binning mode of data collection [42, 43]. The Gaussian fitting procedure, described above for the binding energy spectra, was used to determine the relative intensities of the various transitions at each azimuthal angle ϕ. The experimental momentum profile for a particular transition is obtained by plotting the area under the corresponding fitted peak for each electronic state of the ion as a function of p (i.e. ϕ angle). With this procedure all momentum distributions are automatically placed on the same relative intensity scale. The various theoretical momentum profiles (TMPs) of the valence orbitals were obtained as described in section 3. The finite experimental angular (momentum) resolution ($\Delta p \sim 0.1$ a.u.) is also folded into the TMPs using the GW-PG method [31] and half angles of $\Delta\theta = 0.6°, \Delta\phi = 1.2°$. The experimental and theoretical momentum profiles have been placed on a common intensity scale by normalizing the experimental data for the $1\pi_g$ HOMO orbital to the 199-G(SR-CI) theoretical momentum profile. It should be noted that the 199-G(SR-CI) theoretical momentum profiles are shown assuming unit pole strength. This assignment assumes that the missing pole strength, in excess of the main pole (see Table 4) for each ionization process is contained within the broad envelope of the respective peaks fitted to the binding energy spectra. The same normalization factor obtained in this procedure

is then used for each individual orbital for all experimental and theoretical comparisons.

The theoretical and experimental momentum profiles corresponding to the $1\pi_g$, $1\pi_u$, $3\sigma_g$, $2\sigma_u$ and $2\sigma_g$ orbitals of F_2 are presented in the upper panels of Figs. 3-8 using the above normalization. The corresponding momentum and position density maps calculated for an oriented molecule using the 6-311+G* basis set, which provides a reasonable calculation of the momentum profiles (see next section), are shown in the lower panels of Figs. 3-7. The maps illustrate the bonding and non-bonding characteristics of the respective valence orbitals in the complementary momentum and position representations. The momentum density maps for an oriented fluorine molecule are directly related to the presently reported spherically averaged momentum profiles while the position density maps show the more familiar spatial charge distributions with reference to the nuclei. In addition to the binding energy spectra measured from 16 to 60 eV at $\phi = 0°$ and $\phi = 10°$ (Fig. 1) independent experiments over the binding energy range 14-28 eV (A and B) were also carried out over a wide range of ϕ angles for the three outer valence $1\pi_g$, $1\pi_u$ and $3\sigma_g$ orbitals. In addition a further measurement was also carried out in the inner valence region over a wide range of ϕ angles. In the following discussion comparison between theory and experiment will be made for each orbital in turn.

It can be seen from figure 3 that the A and B sets of measurements for the HOMO $1\pi_g$ orbital are in very good agreement. This doubly degenerate antibonding orbital is mainly due to the out of phase contribution of the 2p lone-pair electrons on the fluorine atoms. Therefore the momentum profile exhibits a "p-type" distribution due to the antisymmetric nature of the wavefunction. The momentum profile is very diffuse and evidently peaks at about 1.1±0.1 a.u. (p_{max}). The high value of p_{max} for this orbital can be related to a contraction in position space and also to the high nodal character of the orbital [60]. The STO-3G calculation predicts a much higher p_{max} at about 1.4 a.u. and this is obviously in disagreement with the experimental data. The improved Hartree-Fock calculations (2 and 3) give very similar results to the momentum profile predicted by the near Hartree-Fock limit (4) calculation in which the large and highly saturated 199-GTO basis set, with diffuse and polarization functions, was used. All these high level Hartree-Fock calculations fit the experimental data reasonably well. The overlap profile from the 199-G(SR-CI) calculation fits the lower momentum points only marginally better than the SCF calculations, although there is apparently still some missing intensity in the low p region even considering the limited statistical precision of the experimental data. Therefore it seems that the effects of electron correlation and relaxation are very small for the $1\pi_g$ momentum profile of F_2. The DFT calculation (curve 6) with the truncated Dunning's basis set (aug-cc-pV5Z) predicts a momentum profile with a p_{max}

at about 1.0 a.u., significantly shifted towards lower momentum compared with the SCF and CI calculations. Some accounting for electron correlation and exchange are also included through the Becke [51] gradient correction to the exchange energy and the Perdew [52] gradient correction to the correlation energy in the DFT calculation. As shown in Table 3, the DFT orbital energy is too small compared to the experimental IP (Table 4) while the SCF orbital energy is too large. Since the long range behaviour of the orbital varies as $\exp(-\sqrt{-2\epsilon}r)$, where ϵ is the orbital energy, this means that the DFT orbital is too diffuse and the SCF orbital is too contracted at large r. A visual examination of Fig. 3 suggests that the DFT calculation may fit the measurements slightly better than the SCF and CI calculations at low momenta and around p_{max}. However, the present experimental statistics do not permit a clear decision in this regard. A more accurate experiment on F_2 would be needed for further detailed comparison and evaluation of the various theoretical models. However, in view of the high reactivity of F_2, such experiments would require differentially pumped microchannelplate detector chambers.

The $1\pi_u$ orbital is also a doubly degenerate orbital. It is mainly due to the in phase combination of the 2p lone-pair electrons of fluorine atoms and thus has a "p-type" distribution. The position density map in figure 4 clearly shows that this is a bonding orbital. The two sets of experimental data for this orbital are reasonably consistent although Expt A does exhibit some scatter. The improved agreement with the experimental data can be seen from curves 1 to 4 in fig. 4 as the quality of the Hartree-Fock calculation is increased. However, there is still appreciably more intensity at momenta below 0.8 a.u. than is predicted by the near Hartree-Fock limit 199-GTO calculation (curve 4). This situation is similar for the outermost π_u orbitals of Br_2 [21] and Cl_2 [20] where less saturated and less diffuse basis sets were used. It was suggested [21] in the case of Br_2 that this missing intensity might be reduced by incorporating diffuse functions in the basis set. In the present work the 199-GTO calculation has both diffuse s and p functions as well as 2f and 1g polarization functions so that the calculation is near to the Hartree-Fock limit. Therefore further expansion of the basis set is unlikely to have any significant additional effect on the momentum profile. The remaining discrepancies between experiment and theory in the low momentum range could then be due to electron correlation effects. It was found that electron correlation effects are very important in the outermost orbital electron distributions of small molecules such as water [6, 10], ammonia [6, 15] and hydrogen fluoride [26]. Although the 199-G(SR-CI) calculation (curve 5), which includes some electron correlation and relaxation effects, does indeed give a somewhat better fit to the experimental data there is still more experimental intensity at momenta below 0.8 a.u. than

is predicted by the 199-G(SR-CI) calculation. It is interesting to note that this discrepancy is apparently removed by the DFT calculation (curve 6) with the non-local approximation and the truncated Dunning basis set (aug-cc-pV5Z). The DFT calculation, which has a lower p_{max} (Table 1), gives the best description of the measured momentum profile of the $1\pi_u$ orbital.

The experimental and calculated momentum profiles of the $3\sigma_g$ orbital of F_2 are shown in figure 5. The $3\sigma_g$ momentum profile displays a mixture of "s-type" and "p-type" character. It was noted previously [6, 7] that the shape of the momentum profiles of such "s-p" mixed orbitals are very sensitive to the quality of basis set functions. The STO-3G (curve 1) and Snyder and Basch (curve 2) calculations give a smaller s/p ratio for the momentum profiles than is observed in the experimental data. Levin et al [61] calculated the momentum profile for the $3\sigma_g$ orbital of F_2 using the basis sets of Wahl [38] and Ransil [62]. The calculated momentum profiles using these simple basis set functions show large "p-type" intensity relative to the "s-type" intensity, similar to the shape of the Snyder and Basch momentum profile given in fig.5. Another calculation of the momentum profile for this orbital was performed by Rozendaal and Baerends [63] using a triple zeta basis set with diffuse 2s and 2p functions and 3d polarization functions. This basis set gives a higher s/p ratio than the observed momentum profile. It is obvious that to correctly calculate the s-p nature of the $3\sigma_g$ orbital both appropriate diffuse functions, and polarization functions are required. The s/p ratio from the high quality Hartree-Fock 199-GTO (curve 4) calculation presented here, using a basis set with both diffuse s and p functions and d,f,g polarization functions, fits the experimental results. The CI calculation (curve 5) using the same basis set as the 199-GTO calculation and including electron correlation and relaxation effects produces a slightly larger s/p ratio than the 199-GTO momentum profile, but both agree equally well with experiment. The DFT calculation predicts a somewhat larger s/p ratio of the momentum profile, similar to the profile given by Rozendaal and Baerends [63].

The first inner valence orbital of F_2 is the antibonding $2\sigma_u$ orbital, due mainly to the out of phase combination of F 2s electrons. This orbital has a "p-type" momentum distribution with the peak at about 0.5 a.u. There is only one set of measurements for this orbital from experiment B. All the calculations from 1 to 6 in figure 6 predict a significantly larger intensity than that measured. It can be seen from the F_2 binding energy spectra in Fig.1 that there is a significant experimental intensity between 25-35 eV and the momentum (angular) profile appears to be a "p-type" distribution, having more intensity in fig.1(a) ($\phi = 10°$) and less intensity in Fig. 1 (b) ($\phi = 0°$). Considering the fact (figures 3 and 4) that the intensities for the $1\pi_g$ and $1\pi_u$ orbitals are already essentially accounted for in their respective momentum

profiles the intensity in this energy range has been ascribed to ionization from the $2\sigma_u$ orbital although it should be noted that $1\pi_u$ intensity is also predicted to occur in this energy region (see Table 4). Accordingly the small intensity in the 25-35 eV energy range was added into the momentum profile of the main $2\sigma_u$ peak. Thus the experimental momentum profile of the $2\sigma_u$ orbital, shown in Fig. 6, includes the intensity of the main peak at 37.3 eV as well as the intensity (about 20 percent of the main peak at 37.3 eV) in the 25-35 eV energy range. However, the experimental intensity is still lower than the theoretical intensity predicted by the various calculations. The missing intensity ($\sim$ 20%) could be located in higher energy regions of the spectrum. This is supported by the Green's function ADC(4) and MRSD-CI calculations (see Table 4). Therefore in order to compare the shape of the $2\sigma_u$ measured momentum profile with theory the MRSD-CI calculation (curve 5) has been multiplied by a factor of 0.8. This scaled CI calculation, represented by the dashed line in figure 6, fits the experimental data quite well.

The inner valence $2\sigma_g$ orbital is mainly derived from the in phase combination of 2s electrons on the fluorine atoms, and thus it has an "s-type" momentum distribution. The CI and Green's function many-body calculations predict many poles distributed over a wide energy range for ionization from this orbital (see Table 4). The measured momentum profile of the main $2\sigma_g$ peak at 42 eV is compared with the calculations in Fig. 7. All the Hartree-Fock, CI and DFT calculations, produce quite similar momentum profiles for this orbital, but obviously overestimate the strength of the transition. In order to compare the shape of the momentum profile the 199-G(MR-CI) calculation has been multiplied by an estimated pole strength of 0.6 and the scaled momentum profile is represented by the dotted line in Fig. 7. Excellent agreement between experiment and theory is then obtained.

It can be seen from the two angle binding energy spectra in figure 1 that the satellite intensity at around 52 eV clearly has an "s-type" distribution and is therefore expected to be derived from the $2\sigma_g$ orbital. Each of the calculations included in the figure also predicts a fairly large $2\sigma_g$ satellite peak in this region (see Table 4). The MRSD-CI calculation places a pole at 52.3 eV which appears to be close to the observed value. The ADC(4) method shows a fairly significant pole around 55 eV and a further pole at 56.2 eV. The experimental momentum profile summed over the energy range of 47-57 eV is compared with 13% of the 199-G(MR-CI) calculation in figure 8 (b). The excellent agreement indicates that the intensity in this energy range is indeed mainly due to ionization from the $2\sigma_g$ orbital and that any contribution from the "p-type" $2\sigma_u$ profile orbital is quite small.

The experimental momentum profile, summed over the 38-60 eV energy range, is com-

pared with the calculations in Fig. 8 (a) and it is clearly dominated by totally symmetric (i.e. "s-type") components. This indicates that the strength over this entire energy region is also mainly from the $2\sigma_g$ orbital, although the many-body calculations (Table 4) do predict a splitting of the $2\sigma_u$ ionization intensity into this binding energy range. It is obvious that the observed intensity in this energy region is significantly lower than the $2\sigma_g$ strength. However a good fit to the experimental data is obtained when, for example for the 199-G(MR-CI)calculation, the $2\sigma_g$ momentum profile is scaled by a factor of 0.75 (represented by the dashed line in figure 8 (a)). This implies that about 25 percent of the $2\sigma_g$ ionization intensity is missing. This discrepancy could be due to the inadequacy of the calculations. However it is more likely, as in the case of the $2\sigma_u$ ionization, that the missing intensity is located in higher energy regions beyond the limit of the present measurements.

5. Comparison of results for F_2, Cl_2, Br_2 and I_2

The complete valence shell binding energy spectra of the four diatomic halogens are each shown in figure 1 of the respective publications for F_2 (present work), Cl_2 [20], Br_2 [21] and I_2 [32]. While the spectra of all four halogens exhibit clear evidence of single dominant poles (at the low resolution of the EMS experiment) for the three outer valence orbitals, the inner valence region becomes increasingly featureless with increase in molecular weight. Whereas in F_2 (see figure 1, present work) clearly resolved separate structures exist for the main intensity from the $2\sigma_u$ and $2\sigma_g$ inner valence orbitals the structures become less clear until in I_2 peaks due to the corresponding $10\sigma_u$ and $10\sigma_g$ orbitals are no longer visible. The density of many-body states at higher energy increases as the independent particle picture of ionization increasingly breaks down with increase in molecular weight. This is understandable in terms of the increased importance of correlation (many-body) and relaxation effects which occur proceeding through the series F_2, Cl_2, Br_2 and I_2 which arises from the lowering of the ionization and excitation energies, the increased importance of quasidegeneracies and the enlarged excitation manifold (d- and f-type excitations e.g.). Many-body Green's Function (MBGF) calculations of the binding energy spectra have been performed at the ADC(4) level for all four molecules (see figure 2, figure 10, figure 8 and figure 8 of the present work and references [20], [21] and [32] respectively). In each case the MBGF calculations underestimate the contributions from higher energy poles in the binding energy spectra. The similar behavior was observed in the case of the hydrogen halides [18, 19, 26, 33].

A consideration of the respective momentum profiles shows that SCF calculations with

reasonably large basis sets provide quite good quantitative descriptions of the experimental results for the two outermost valence orbitals (π_g and π_u symmetry) of all four diatomic halogens. For the two inner valence orbitals (σ_u and σ_g symmetry) the shape of the profiles is well predicted although the increased intermingling of the poles from the two symmetries and the limited energy resolution precludes a separate analysis of the σ_u and σ_g integrated profiles except in the case of F_2. However the situation is rather different in the case of the experimental (XMP) and theoretical (TMP) momentum profiles for the third valence orbital ($3\sigma_g(F_2)$, $5\sigma_g(Cl_2)$, $8\sigma_g(Br_2)$, and $11\sigma_g(I_2)$), which all exhibit mixed "s-p" character (see Fig. 9). The XMP's of these strongly bonding orbitals (see density maps in respective papers) show a trend of a significantly increasing "p" contribution relative to "s" in going from F_2 to Cl_2, to Br_2, to I_2. This is consistent with other group bonding trends such as for example in the hydrides of group VIA. In this case the bond angles decrease down the series, $H_2O(104.5°)$, $H_2S(93.3°)$, $H_2Se(91.0°)$ and $H_2Te(89.5°)$, reflecting the bonding changes from essentially sp^3 to mainly pure p character in terms of the hybridization model description. Similar behaviour is also found in comparing the HOMO XMP's for NX_3 [10] and PX_3 [64] molecules (where X = H, F or CH_3).

Acknowledgements

This project received financial support from The Australian Research Council (ARC), The Flinders University of South Australia, The Natural Sciences and Engineering Research Council of Canada, and The National Science Foundation (USA). We would also like to thank Dr. T. O'Donnell of Melbourne University for providing several low pressure samples of fluorine gas and for helpful information concerning safe sample handling and disposal of F_2. Three of us (CEB, AS and WVN) gratefully acknowledge financial support and hospitality during visits to The Flinders University of South Australia. One of us (MJB) also thank the ARC for provision of a QE2 Fellowship and support grant.

References

[1] I.E. McCarthy and E. Weigold. Phys. Rep. **27C** (1976) 275.

[2] C.E. Brion. Int. J. Quantum Chem. **29** (1986) 1397, and references therein.

[3] I.E. McCarthy and E. Weigold. Rep. Prog. Phys. **51** (1988) 299.

[4] I. McCarthy and E. Weigold. *Rep. Prog. Phys.* **91** (1991) 789, and references therein.

[5] C.E. Brion. In *Correlations and Polarization in Electronic and Atomic Collisions and (e,2e) Reactions* , Inst. Phys. Conf. Series **122** (1992) 171, Institute of Physics (Bristol).

[6] C.E. Brion. In *The Physics of Electronic and Atomic Collisions*, Eds. T. Andersen et al., American Institute of Physics Press, New York (1993) 350, and references therein.

[7] A.O. Bawagan and C.E. Brion. Chem. Phys. Lett. **137** (1987) 573, Chem. Phys., **123** (19SS) 51.

[8] D. Feller, C.M. Boyle, and E.R. Davidson. J. Chem. Phys., **86** (1987) 3424.

[9] I.N. Levine. Quantum Chemistry: Prentice Hall, NJ, (1991) 474.

[10] A.O. Bawagan, C.E. Brion, E.R. Davidson, and D. Feller. Chem. Phys. **113** (1987) 19.

[11] P. Duffy, D.P. Chong, M.E. Casida, and D.R. Salahub. Phys. Rev. A **50** (1994) 4704, and references therein.

[12] B.P. Hollebone, J.J. Neville, Y. Zheng, C.E. Brion, Y. Wang, and E.R. Davidson. Chem. Phys., **196** (1995) 13.

[13] Y. Zheng, J.J. Neville, C.E. Brion, Y. Wang, and E.R. Davidson. Chem. Phys., **188** (1994) 109.

[14] Y. Zheng, J.J. Neville, and C.E. Brion. Science, **270** (1995) 786.

[15] A.O. Bawagan, R. Muller-Fiedler, C.E. Brion, E.R. Davidson, and C. Boyle. Chem. Phys., **120** (1988) 335.

[16] K.T. Leung and C.E. Brion. Chem. Phys., **96** (1985) 241.

[17] J.P.D. Cook, M.G. White, C.E. Brion, W. Domcke, J. Schirmer, L.S. Cederbaum, and W. von Niessen. J. Elec. Spectrosc. Relat. Phenom., **22** (1981) 261.

[18] B.P. Hollebone, C.E. Brion, E.R. Davidson, and C. Boyle. Chem. Phys., **173** (1994) 193.

[19] C.E. Brion, I.E. McCarthy, I.H. Suzuki, E. Weigold, G.R.J. Williams, K.L. Bedford, A.B. Kunz, and E. Weidman. J. Elec. Spectrosc. Relat. Phenom., **27** (1982) 83.

[20] L. Frost, A.M. Grisogono, I.E. McCarthy, E. Weigold, C.E. Brion, A.O. Bawagan, P.K. Mukherjee, W. von Niessen, M. Rosi, and A. Sgamellotti. Chem. Phys., **113** (1987) 1.

[21] L. Frost, A.M. Grisogono, E. Weigold, C.E. Brion, A.O. Bawagan, P. Tomasello, and W. von Niessen. Chem. Phys., **119** (1988) 253.

[22] S.J. Desjardins, A.D.O. Bawagan, Z.F. Liu, K.H. Tan, Y. Wang, and E.R. Davidson. J. Chem. Phys., **102** (1995) 6385.

[23] K.T. Leung and C.E. Brion. J. Elec. Spectrosc. Relat. Phenom., **35** (1986) 327.

[24] K.T. Leung. Theoretical Models of Chemical Bonding, Part 3; Z.B. Maksic, Ed., Springer Verlag Berlin, (1991) 339.

[25] S.A.C. Clark, T.J. Reddish, C.E. Brion, E.R. Davidson, and R.F. Frey. Chem. Phys., **143** (1990) 1.

[26] B.P. Hollebone, Y. Zheng, C.E. Brion, E.R. Davidson, and D. Feller. Chem. Phys., **171** (1993) 303.

[27] S.W. Braidwood, M.J. Brunger, D.A. Kerovalov, and E. Weigold. J. Phys., **B 26** (1993) 1655.

[28] S.A.C. Clark, E. Weigold, C.E. Brion, E.R. Davidson, R.F. Frey, C.M. Boyle, W. von Niessen, and J. Schirmer. Chem. Phys., **134** (1989) 229.

[29] S.A.C. Clark, C.E. Brion, E.R. Davidson, and C. Boyle. Chem. Phys., **136** (1989) 55.

[30] C.L. French, C.E. Brion, and E.R. Davidson. Chem. Phys., **122** (1988) 247.

[31] P. Duffy, C.E. Brion, M.E. Casida, and D.P. Chong. Chem. Phys., **159** (1992) 347.

[32] A.M. Grisogono, R. Pascual, E. Weigold, C.E. Brion, and W. von Niessen. Chem. Phys., **124** (1988) 121.

[33] C.E. Brion, S.T. Hood, I.H. Suzuki, E. Weigold, and G.R.J.Williams. J. Elec. Spectrosc. Relat. Phenom., **21** (1980) 71.

[34] P. Duffy. Ph.D thesis, University of British Columbia, (1995).

[35] J.P.D. Cook, R. Pascual, E. Weigold, W. von Niessen, and P. Tomasello. Chem. Phys., **141** (1990) 211.

[36] I.H. Suzuki, E. Weigold, and C.E. Brion. J. Elec. Spectrosc. Relat. Phenom., **20** (1980) 289.

[37] J. Rolke, N. Cann, Y. Zheng, B.P. Hollebone, C.E. Brion, Y. Wang, and E.R. Davidson. Chem. Phys., **201** (1995) 1.

[38] A.C. Wahl. J. Chem. Phys., **41** (1964) 2600.

[39] G. Bieri, L. Asbrink, and W. von Niessen. J. Elec. Spectrosc. Relat. Phenom., **23** (1981) 281.

[40] M.R.A. Blomberg and P.E.M. Siegbahn. Chem. Phys. Lett., **81** (1981) 4.

[41] M.E. Casida. Phys. Rev., **A 51** (1995) 2005.

[42] J.P.D. Cook, I.E. McCarthy, A.T. Stelbovics, and E. Weigold. J. Phys. **B 17** (1984) 2339.

[43] O. Samardzic, E. Weigold, W. von Niessen, V.G. Zakozewski, and M.J. Brunger. Chem. Phys. **182** (1994) 361.

[44] W.J. Hehre, R.F. Stewart, and J.A. Pople. J. Chem. Phys., **51** (1969) 2657.

[45] L.C. Snyder and H. Basch. *Molecular Wavefunctions and Properties* (John Wiley and Sons, 1972).

[46] R. Krishnan, M.J. Frisch, and J.A. Pople. J. Chem. Phys., **72** (1980) 4244.

[47] H. Partridge. *Near-Hartree-Fock quality GTO basis sets for the first- and second-row atoms, NASA Technical Memorandum* 101044 (1989).

[48] S.C. Racine and E.R. Davidson. J. Phys. Chem., **97** (1993) 6367, the exponents for the d set are (10.83, 3.868, 1.381, 0.493) and the f set are (6.033, 2.011, 0.670).

[49] W.J. Hunt and W. A. Goddard III. Chem. Phys. Lett., 3 (1969) 414.

[50] MELD is a package of electronic structure codes developed by. L.E. McMurchie, S.T. Elbert. S.R. Langhoff, and E.R. Davidson and was extensively modified by D. Feller and D.C. Rawlings.

[51] A.D. Becke. Phys. Rev. A 38 (1988) 3098.

[52] J.P. Perdew. Phys. Rev. A 33 (1986) 8822.

[53] T.H. Dunning Jr. J. Chem. Phys., 90 (1989) 1007.

[54] D.R. Salahub, R. Fournier, P. Mlanarski, I. Papai, A. St. Amant, and J. ushio. *Density Functional Methods in Chemistry* Eds. J. Labanowski and J. Andzelm (Springer, V New York, 1991) p. 77.

[55] A.B. Cornford, D.C. Frost, C.A. McDowell, J.L. Ragle, and I.A. Stenhouse. J. Chem. Phys., 54 (1971) 2651.

[56] L.S. Cederbaum, G. Hohlneicher, and W. von Niessen. Mol. Phys., 26 (1973) 1405.

[57] P. Weightman and T.D. Thomas. J. Chem. Phys., 78 (1983) 1652.

[58] J. Schirmer, L.S. Cederbaum, and O. Walter. Phys. Rev., A 28 (1983) 1237.

[59] C. Salez and A. Veillard. Theor. Chim. Acta, 11 (1968) 441.

[60] A.O. Bawagan, C.E. Brion, M.A. Coplan, J.A. Tossell, and J.H. Moore. Chem. Phys., 110 (1986) 153.

[61] V.G. Levin, V.G. Neudatchin, A.V. Pavlitchenkov, and Yu.F. Smirnov. J. Chem. Phys., 63 (1975) 1541.

[62] B.Y. Ransil. Rev. Mod. Phys., 32 (1960) 245.

[63] A. Rozendaal and E.J. Baerends. Chem. Phys., 87 (1984) 263.

[64] J. Rolke and C.E. Brion. Chem. Phys., submitted 1995.

[65] T.H. Spurling and E.A. Mason. J. Chem. Phys., 46 (1967) 322.

[66] J.F. Ely, H.J.M. Hanley, and G.C. Straty. J. Chem. Phys., 59 (1973) 859.

Table 1: Basis sets and calculated properties for F_2

#[a]	Basis type	Reference	Basis set	Total energy (hartree)	Θ^{b}_{zz} (au)	P_{MAX}(au)[c]	R(Å)
1	HF STO-3G	[44]	Gaussian [2s1p]	-195.9658	0.1660	1.47	1.418
2	HF S&B	[45]	Gaussian [4s1p]	-198.6932	0.1833	1.20	1.418
3	HF 6-311+G*	[46]	Gaussian [5s4p1d]	-198.7312	0.4064	1.19	1.418
	HF aug-cc-PV5Z[d]	[53],e	Gaussian [7s6p5d]	-198.7680	0.5486	1.17	1.418
	HF aug-cc-PV5Z[d]	[53]	Gaussian [7s6p5d4f]	-198.7720	0.5052	1.17	1.418
4	HF 199-GTO	f	Gaussian [12s8p4d3f1g]	-198.7733	0.4912	1.17	1.41193
5	CI 199-G(CI)[g]	f	Gaussian [12s8p4d3f1g]	-199.3300	0.6659	1.14	1.41193
6	DFT-PV5Z-BP	f,e	Gaussian [7s6p5d]	-199.6202	0.7062	1.04	1.418
	Experimental			-199.529[h]	1.0-1.3 [65] 0.56 [66]	1.1±0.1	

[a] These numbers refer to the calculations in section 3 and figures 3-8.

[b] In comparing with experimental value of the quadrupole moment (Θ_{zz}) it should be noted that the calculations are at the equilibrium geometry (i.e. for a non-vibrating and non-rotating molecule).

[c] Momentum value for maximum in the $1\pi_g$ momentum profile. From Fig.3.

[d] These two calculations were performed to investigate the effects of f function truncation in the basis set used in the DFT calculations, i.e. #6. See text for details.

[e] This is the Dunning basis set [53] with the truncation of f functions, see text.

[f] These calculations were developed in the course of the present work.

[g] Frozen 1s core.

[h] Experimental non-relativistic, non-vibrating energy.

Table 2. Total SCF and MP2 correlation energies with the constructed basis set[a].

	Basis	SCF	MP2
F	20s,14p	-99.409346	
	12s, 8p	-99.409346	
	Numerical	-99.409349	
R = 2.668 Bohr			
F_2	12s,8p,4d,3f,1g/3s,3p,3d	-198.773336	-0.66466
F_2	12s,8p,4d,3f,1g	-198.773329	-0.65505
F_2	12s,8p,4d,3f	-198.773088	-0.66426
F_2	Numerical	-198.7741	

R = 2.66816076 Bohr

	ROHF	MCSCF	MRMP2	E_c	ΔE (eV)
F_2	-198.773336	-198.850067	-199.446179	-0.67284	-
F_2^+	-198.462209	-198.317600	-198.863310	-0.40110	15.86
F_2^{++}	-197.067757	-197.344771	-197.828503	-0.76075	44.02

[a]Only pure *l* functions were used. E_c is the correlation energy relative to ROHF.

Table 3. Occupied orbital and IVO energies[a] (eV).

	199GTO	5s3p1d	5s4p1d	6-311+G*	7s6p5d	7s6p5d(DFT)	NHF[b]
$1\sigma_g$	-719.14	-719.23	-719.33	-719.41	-719.18	-663.59	-719.14
$1\sigma_u$	-719.14	-719.22	-719.32	-719.41	-719.17	-663.60	-719.14
$2\sigma_g$	-48.02	-47.75	-48.04	-48.19	-47.97	-33.98	-48.02
$2\sigma_u$	-40.75	-40.90	-40.72	-40.98	-40.82	-27.76	-40.75
$1\pi_u$	-22.08	-21.92	-22.09	-22.18	-22.04	-12.91	-22.08
$3\sigma_g$	-20.45	-20.22	-20.50	-20.49	-20.44	-15.52	-20.46
$1\pi_g$	-18.15	-18.24	-18.18	-18.36	-18.19	-9.58	-18.15
$3\sigma_u$	-31.11	-31.50	-31.23				
$4\sigma_g$	-11.04	-1.61	-7.63				
$2\pi_u$	-8.68	-4.11	-8.33				
$4\sigma_u$	-8.03	-2.78	-7.56				
$5\sigma_g$	-6.29	0.01	-5.50				
$1\delta_g$	-5.92	32.00	37.20				
$2\pi_g$	-5.79	0.63	-4.95				
$6\sigma_g$	-4.98	33.73	9.80				

[a]IVO's calculated by diagonalizing the $F_2^{++}\ ^3\Sigma_g^-$ Fock operator formed using $F_2\ ^1\Sigma_g^+$ orbitals over the F_2 virtual space.
[b]Numerical Hartree-Fock.

Table 4: Experimental and theoretical ionization potentials (eV) and pole strengths (in parentheses) for molecular fluorine

		Experiment			Theory		
Peak[a]	Orbital	EMS	PES[b]	SCF[c]	MRSD-CI[d]	Direct-CI[e]	GF-ADC(4)[f]
1	$1\pi_g$	15.8	15.87	18.14	15.35(0.805)		15.48(0.877)
					27.86(0.002)		31.37(0.027)
					32.03(0.004)		33.39(0.005)
					34.21(0.006)		39.93(0.008)
					41.19(0.003)		40.80(0.006)
2	$1\pi_u$	18.9	18.80	22.07	18.58(0.715)		18.61(0.806)
					24.49(0.012)		23.86(0.014)
					29.37(0.012)		28.61(0.009)
					31.24(0.062)		31.06(0.026)
					32.99(0.004)		32.34(0.012)
					37.95(0.002)		38.63(0.005)
					38.23(0.003)		43.23(0.005)
							46.44(0.006)
3	$3\sigma_g$	20.9	21.10	20.45	20.91(0.824)	20.48(0.903)	20.65(0.856)
					22.49(0.002)		21.17(0.035)
					28.84(0.018)		22.63(0.008)
					33.22(0.004)		42.55(0.003)
					41.57(0.006)		45.76(0.002)
							47.76(0.008)
							50.12(0.002)

(continued on page 32)

(continued Table 4)

4	$2\sigma_u$	25.35		40.73	29.60(0.011)		
					32.55(0.066)	28.89(0.036)	28.51(0.035)
					33.83(0.003)	31.70(0.064)	31.52(0.025)
					36.62(0.019)	32.89(0.003)	32.31(0.006)
		37.3	37.47[c]		37.67(0.644)	37.36(0.725)	37.52(0.787)
					38.47(0.022)		38.85(0.012)
					43.22(0.006)		41.42(0.005)
					44.87(0.008)		43.40(0.003)
							45.09(0.005)
							48.13(0.003)
							58.45(0.004)
							58.94(0.008)
							59.39(0.017)
5	$2\sigma_g$			46.00		20.48(0.002)	22.63(0.003)
						27.77(0.005)	31.31(0.004)
					32.98(0.004)		39.51(0.011)
					42.24(0.003)		40.15(0.003)
					42.77(0.136)		41.23(0.008)
		41.2	41.75[c]		42.97(0.505)	42.07(0.850)	42.55(0.696)
					47.67(0.002)		45.76(0.003)
					48.29(0.017)		48.94(0.003)
					48.69(0.002)		49.10(0.017)
					50.10(0.003)		49.58(0.004)
					50.83(0.002)		50.12(0.002)
					51.24(0.002)		51.98(0.010)
					51.35(0.002)		52.07(0.009)
					53.11(0.008)		52.26(0.003)
					53.19(0.002)		53.66(0.005)
							54.51(0.005)
		52					55.60(0.076)
							56.20(0.035)
							56.90(0.003)

[a] See Fig.3.
[b] ref. [39].
[c] ref. [57].
[d] SCF and MRSD-CI calculations were carried out at Indiana University using the 199-GTO Gaussian basis set.
[e] Calculated at Universita di Perugia, Italy, using a direct-CI method and Dunning's [5s3p1d] basis set.
[f] Calculated at Technische Universitat, Braunschweig, Germany, using the ADC(4) Green's function method and a [5s4p1d] Gaussian basis set.

Table 5. Primary hole single root MRSDCI calculations[a].

	State	Energy[c]	Diff[b]	S_ν^2[d]	Dominant orb.[e]		Dominant Configurations[f]	Coeff.[g]
1	Σ_g^+	-198.555	21.09	.814	1.00[3]	-.02[9]	$3\sigma_g(-1)$	.939
1	Π_{ru}	-198.632	18.99	.748	1.00[1]	.01[2]	$1\pi_{ru}(-1)$	.878
							$3\sigma_g(-1)3\sigma_u(1)1\pi_{ug}(-1)$	.342
1	Π_{ug}	-198.748	15.84	.802	1.00[1]	.01[2]	$1\pi_{rg}(-1)$	.910

[a]Perturbation selection done with threshold of 1E-7. Orbitals: Improved virtual orbitals.
[b]Difference from corresponding neutral F_2 energy in eV.
[c]CI energy of F_2^+ in Hartrees. The comparable neutral F_2 energy was -199.330.
[d]Pole strength.
[e]Dominant terms of the expansion of the normalized Dyson orbital in terms of neutral F_2 occupied and improved virtual orbitals of the appropriate symmetry. For example, the Π_{ru} entry indicates a Dyson orbital 1.00 $(1\pi_{ru})$ + .01$(2\pi_{ru})$.
[f]Dominant configuration in the CI for the F_2^+ state indicated in particle-hole notation relative to the SCF configuration of F_2.
[g]Absolute value of coefficient of dominant configuration. When more than one spin coupling is possible, this gives the square root of the sum of the squares of all spin eigenfunctions with this orbital occupancy.

Table 6. $^2\Sigma_g^+$ states of F_2^+[a].

	State	Energy	Diff	S_ν^2	Dominant orb.		Dominant Configurations	Coeff.
1[b]	Σ_g^+	-199.294					SCF	.947
							$3\sigma_g(-2)3\sigma_u(2)$	.182
1	Σ_g^+	-198.525	20.91	.824	1.00[3]	-.02[10]	$3\sigma_g(-1)$	.939
2	Σ_g^+	-198.467	22.49	.002	.97[3]	-.07[10]	$1\pi_{ru}(-1)3\sigma_u(1)1\pi_{rg}(-1)$	.673
							$1\pi_{ru}(-1)3\sigma_u(1)1\pi_{rg}(-1)$	.673
3	Σ_g^+	-198.234	28.84	.016	.87[3]	-.01[10]	$1\pi_{ru}(-1)3\sigma_u(1)1\pi_{rg}(-1)$	.517
							$1\pi_{ru}(-1)3\sigma_u(1)1\pi_{rg}(-1)$	.517
							$3\sigma_g(-1)3\sigma_u(2)1\pi_{rg}(-2)$	.408
							$3\sigma_g(-1)3\sigma_u(2)1\pi_{rg}(-2)$	.408
4	Σ_g^+	-199.082	32.96	.004	.90[2]	.43[3]	$3\sigma_g(-1)1\pi_{ru}(-2)3\sigma_u(2)$	.441
							$3\sigma_g(-1)1\pi_{ru}(-2)3\sigma_u(2)$	.441
							$3\sigma_g(-1)3\sigma_u(2)1\pi_{rg}(-2)$	.402
							$3\sigma_g(-1)3\sigma_u(2)1\pi_{rg}(-2)$	.402
5	Σ_g^+	-197.988	35.53	.001	.98[2]	-.18[3]	$4\sigma_g(1)1\pi_{rg}(-2)$	.565
							$4\sigma_g(1)1\pi_{rg}(-2)$	.565
6	Σ_g^+	-197.846	39.40	.000	.98[2]	-.14[4]	$1\pi_{ru}(-1)4\sigma_u(1)1\pi_{rg}(-1)$	.635
							$1\pi_{ru}(-1)4\sigma_u(1)1\pi_{rg}(-1)$	.635
7	Σ_g^+	-197.834	39.73	.000	.97[2]	-.22[3]	$1\delta_g(1)1\pi_{ug}(-1)1\pi_{ug}(-1)$	.816
							$1\pi_{rg}(-1)1\pi_{ru}(-1)1\delta_g(1)$	.351
8	Σ_g^+	-197.813	40.30	.000	.96[2]	-.28[3]	$5\sigma_g(1)1\pi_{rg}(-2)$	.495
							$5\sigma_g(1)1\pi_{rg}(-2)$	.495
9	Σ_g^+	-197.807	40.46	.000	.93[2]	-.15[3]	$1\delta_g(1)1\pi_{ug}(-2)$	.532
							$1\delta_g(1)1\pi_{ug}(-2)$	.532
10	Σ_g^+	-197.778	41.25	.001	1.00[2]	-.02[3]	$2\pi_{ru}(1)3\sigma_u(1)1\pi_{rg}(-2)1\pi_{rg}(-1)$	.563
							$2\pi_{ru}(1)3\sigma_u(1)1\pi_{rg}(-1)1\pi_{rg}(-2)$	.563
11	Σ_g^+	-197.766	41.57	.005	1.00[2]	-.09[3]	$7\sigma_g(1)1\pi_{rg}(-2)$	.561
							$7\sigma_g(1)1\pi_{rg}(-2)$	.561
12	Σ_g^+	-197.750	42.01	.001	1.00[2]	-.02[3]	$4\sigma_g(1)3\sigma_u(2)1\pi_{rg}(-2)1\pi_{rg}(-2)$	.580
							$2\pi_{ru}(1)3\sigma_u(1)1\pi_{rg}(-2)1\pi_{ug}(-1)$	.313

							$2\pi_{xu}(1)3\sigma_u(1)1\pi_{xg}(-1)1\pi_{yg}(-2)$	.313
							$4\sigma_g(1)1\pi_{xu}(-2)3\sigma_u(2)1\pi_{yg}(-2)$	.303
							$4\sigma_g(1)1\pi_{yu}(-2)3\sigma_u(2)1\pi_{xg}(-2)$	.303
13	Σ_g^+	-197.741	42.24	.003	1.00[2]	-.03[3]	$2\pi_{yu}(1)3\sigma_u(1)1\pi_{xg}(-2)1\pi_{yg}(-1)$	.461
							$2\pi_{xu}(1)3\sigma_u(1)1\pi_{yg}(-1)1\pi_{xg}(-2)$	.461
							$4\sigma_u(1)3\sigma_u(2)1\pi_{xg}(-2)1\pi_{yg}(-2)$	.385
14	Σ_g^+	-197.722	42.77	.138	1.00[2]	-.07[3]	$2\delta_g(1)1\pi_{xg}(-1)1\pi_{yg}(-1)$	.736
							$2\sigma_g(-1)$	.372
15	Σ_g^+	-197.715	42.97	.505	1.00[2]	-.07[3]	$2\sigma_g(-1)$	.713
							$2\delta_g(1)1\pi_{xg}(-1)1\pi_{yg}(-1)$	.359
							$3\sigma_g(-1)2\sigma_u(-1)3\sigma_u(1)$	.356
16	Σ_g^+	-197.613	45.74	.000	.95[2]	-.22[4]	$4\sigma_u(1)1\pi_{xu}(-2)$	.459
							$4\sigma_u(1)1\pi_{yu}(-2)$	.459
							$3\sigma_g(-1)4\sigma_u(1)1\pi_{yu}(-1)3\sigma_u(1)1\pi_{yg}(-1)$	.316
							$3\sigma_g(-1)4\sigma_u(1)1\pi_{xu}(-1)3\sigma_u(1)1\pi_{xg}(-1)$	.316
17	Σ_g^+	-197.542	47.67	.002	1.00[2]	-.05[3]	$3\sigma_g(-1)4\sigma_u(1)1\pi_{xu}(-1)3\sigma_u(1)1\pi_{xg}(-1)$	.453
							$3\sigma_g(-1)4\sigma_u(1)1\pi_{yu}(-1)3\sigma_u(1)1\pi_{yg}(-1)$	.453
							$1\pi_{xu}(-1)1\pi_{yu}(-1)2\pi_{yg}(1)3\sigma_u(1)1\pi_{xg}(-1)$	.357
							$1\pi_{xu}(-1)2\pi_{xu}(1)1\pi_{yu}(-1)3\sigma_u(1)1\pi_{yg}(-1)$	.357
18	Σ_g^+	-197.539	47.75	.000	.99[2]	-.17[3]	$3\sigma_g(-1)4\sigma_u(1)1\pi_{xu}(-1)3\sigma_u(1)1\pi_{xg}(-1)$	.486
							$3\sigma_g(-1)4\sigma_u(1)1\pi_{xu}(-1)3\sigma_u(1)1\pi_{yg}(-1)$	.486
							$1\pi_{xu}(-1)1\pi_{yu}(-1)2\pi_{yg}(1)3\sigma_u(1)1\pi_{xg}(-1)$	.334
							$1\pi_{xu}(-1)2\pi_{xu}(1)1\pi_{yu}(-1)3\sigma_u(1)1\pi_{yg}(-1)$	.334
19	Σ_g^+	-197.519	48.29	.017	.99[2]	-.10[3]	$3\sigma_g(-1)1\pi_{xu}(-2)3\sigma_u(2)$	.344
							$3\sigma_g(-1)1\pi_{yu}(-2)3\sigma_u(2)$	.344
							$3\sigma_g(-1)2\sigma_u(-1)3\sigma_u(1)$	.311
20	Σ_g^+	-197.504	48.69	.001	.99[2]	.16[3]	$1\pi_{xu}(-1)4\sigma_u(1)1\pi_{yg}(-1)$	.489
							$1\pi_{yu}(-1)4\sigma_u(1)1\pi_{xg}(-1)$	.489
21	Σ_g^+	-197.497	48.89	.002	.97[2]	-.22[3]	$1\pi_{xu}(-1)2\pi_{xu}(1)1\pi_{yu}(-1)3\sigma_u(1)1\pi_{yg}(-1)$	.423
							$1\pi_{xu}(-1)1\pi_{yu}(-1)2\pi_{xg}(1)3\sigma_u(1)1\pi_{xg}(-1)$	.423
							$1\pi_{xu}(-2)2\pi_{xg}(1)3\sigma_u(1)1\pi_{yg}(-1)$	.317
							$2\pi_{xu}(1)1\pi_{yu}(-2)3\sigma_u(1)1\pi_{yg}(-1)$	.317
22	Σ_g^+	-197.492	49.01	.000	.72[3]	-.39[16]	$1\pi_{xu}(-1)1\pi_{yu}(-1)2\pi_{yu}(1)3\sigma_u(1)1\pi_{xg}(-1)$	.434
							$1\pi_{yu}(-1)2\pi_{xu}(1)1\pi_{xu}(-1)3\sigma_u(1)1\pi_{yg}(-1)$	.434
							$1\pi_{xu}(-2)2\pi_{yu}(1)3\sigma_u(1)1\pi_{xg}(-1)$	.368
							$2\pi_{xu}(1)1\pi_{yu}(-2)3\sigma_u(1)1\pi_{xg}(-1)$	.368
23	Σ_g^+	-197.487	49.15	.001	1.00[2]	-.03[11]	$3\sigma_g(-1)4\sigma_u(1)1\pi_{xu}(-1)3\sigma_u(1)1\pi_{xg}(-1)$	.401
							$3\sigma_g(-1)4\sigma_u(1)1\pi_{yu}(-1)3\sigma_u(1)1\pi_{yg}(-1)$	.401
							$1\pi_{xu}(-1)1\pi_{yu}(-1)2\pi_{yg}(1)3\sigma_u(1)1\pi_{xg}(-1)$	.381

							$1\pi_{xu}(-1)2\pi_{xu}(1)1\pi_{yu}(-1)3\sigma_u(1)1\pi_{yg}(-1)$	.381
							$1\pi_{xu}(-1)2\pi_{yu}(1)1\pi_{yu}(-1)3\sigma_u(1)1\pi_{xg}(-1)$	.412
							$1\pi_{xu}(-1)1\pi_{yu}(-1)2\pi_{xg}(1)3\sigma_u(1)1\pi_{xg}(-1)$	.412
							$3\sigma_g(-1)4\sigma_u(1)1\pi_{xu}(-1)3\sigma_u(1)1\pi_{xg}(-1)$	.385
							$3\sigma_g(-1)4\sigma_u(1)1\pi_{xu}(-1)3\sigma_u(1)1\pi_{yg}(-1)$	.385
25	Σ_g^+	-197.479	49.38	.001	1.00[2]	-.02[12]	$4\sigma_g(1)1\pi_{xu}(-1)1\pi_{xu}(-1)3\sigma_u[2]1\pi_{xg}(-1)1\pi_{yg}(-1)$	.553
							$1\pi_{xu}(-1)1\pi_{yu}(-1)1\delta_g(1)$	.464
26	Σ_g^+	-197.477	49.45	.001	.99[2]	-.11[3]	$1\pi_{xu}(-1)1\pi_{yu}(-1)1\delta_g(1)$	.532
							$4\sigma_g(1)1\pi_{xu}(-1)1\pi_{xu}(-1)3\sigma_u[2]1\pi_{xg}(-1)1\pi_{yg}(-1)$	.492
27	Σ_g^+	-197.461	49.87	.000	.94[2]	-.29[3]	$1\pi_{yu}(-1)5\sigma_u(1)1\pi_{yg}(-1)$	.431
							$1\pi_{xu}(-1)5\sigma_u(1)1\pi_{xg}(-1)$	.431
							$1\pi_{xu}(-1)2\pi_{xu}(1)1\pi_{yu}(-1)3\sigma_u(1)1\pi_{yg}(-1)$	.328
							$1\pi_{xu}(-1)1\pi_{yu}(-1)2\pi_{xg}(1)3\sigma_u(1)1\pi_{xg}(-1)$	.328
28	Σ_g^+	-197.458	49.94	.000	.91[2]	-.38[3]	$1\pi_{xu}(-1)5\sigma_u(1)1\pi_{xg}(-1)$	.454
							$1\pi_{yu}(-1)5\sigma_u(1)1\pi_{xg}(-1)$	.454
							$1\pi_{xu}(-1)2\pi_{xu}(1)1\pi_{xu}(-1)3\sigma_u(1)1\pi_{yg}(-1)$	.317
							$1\pi_{xu}(-1)1\pi_{yu}(-1)2\pi_{yu}(1)3\sigma_u(1)1\pi_{xg}(-1)$	.317
29	Σ_g^+	-197.453	50.09	.000	.84[3]	-.16[13]	$9\sigma_g(1)1\pi_{xg}(-2)$	.574
							$9\sigma_g(1)1\pi_{yg}(-2)$	.574
30	Σ_g^+	-197.452	50.10	.003	1.00[2]	-.04[13]	$1\delta_g(1)1\pi_{xu}(-2)$	.492
							$1\delta_g(1)1\pi_{yu}(-2)$	.492
							$3\sigma_g(-1)1\delta_g(1)1\pi_{yu}(-1)3\sigma_u(1)1\pi_{yg}(-1)$	.325
							$3\sigma_g(-1)1\delta_g(1)1\pi_{xu}(-1)3\sigma_u(1)1\pi_{xg}(-1)$	.325
31	Σ_g^+	-197.447	50.25	.000	.95[2]	-.30[3]	$3\sigma_g(-1)3\sigma_u(1)4\sigma_u(1)1\pi_{yg}(-2)$	.464
							$3\sigma_g(-1)3\sigma_u(1)4\sigma_u(1)1\pi_{xg}(-2)$	.464
32	Σ_g^+	-197.436	50.55	.000	.54[10]	-.46[13]	$8\sigma_u(1)1\pi_{xg}(-2)$	.470
							$8\sigma_u(1)1\pi_{yg}(-2)$	.470
33	Σ_g^+	-197.425	50.83	.002	.96[2]	-.23[3]	$3\sigma_g(-1)2\sigma_u(-1)3\sigma_u(1)$	.377
							$4\sigma_g(1)1\pi_{xu}(-1)1\pi_{yu}(-1)3\sigma_u[2]1\pi_{xg}(-1)1\pi_{yg}(-1)$	.310
34	Σ_g^+	-197.423	50.90	.000	.92[2]	.36[3]	$4\sigma_g(1)1\pi_{xu}(-1)1\pi_{xu}(-1)3\sigma_u[2]1\pi_{xg}(-1)1\pi_{yg}(-1)$	.561
							$4\sigma_u(1)1\pi_{xu}(-2)3\sigma_u[2]1\pi_{yg}(-2)$	.340
							$4\sigma_u(1)1\pi_{yu}(-2)3\sigma_u[2]1\pi_{xg}(-2)$	.340
35	Σ_g^+	-197.416	51.10	.001	.85[2]	-.46[3]	$3\sigma_g(-1)2\sigma_u(-1)3\sigma_u(1)$	.374
							$3\sigma_g(-1)2\sigma_u(-1)3\sigma_u(1)$	.463
36	Σ_g^+	-197.410	51.24	.002	.90[2]	-.38[3]	$1\pi_{xu}(-1)2\pi_{xu}(1)1\pi_{xu}(-1)3\sigma_u(1)1\pi_{yg}(-1)$	.345
							$1\pi_{xu}(-1)1\pi_{yu}(-1)2\pi_{yu}(1)3\sigma_u(1)1\pi_{xg}(-1)$	.346
37	Σ_g^+	-197.407	51.35	.002	.77[2]	-.51[3]	$3\sigma_g(-1)1\pi_{yu}(-1)2\pi_{yu}(1)$	.356
							$3\sigma_g(-1)1\pi_{xu}(-1)2\pi_{xu}(1)$	.356

38	Σ_g^+	-197.382	52.02	.000	.93[3]	-.16[13]	$3\sigma_g(-1)1\pi_{xg}(-1)1\delta_g(1)3\sigma_u(1)1\pi_{yg}(-1)$	.522
							$3\sigma_g(-1)1\pi_{yg}(-1)1\delta_g(1)3\sigma_u(1)1\pi_{xg}(-1)$	.522
							$3\sigma_g(-1)1\delta g(1)1\pi_{xu}(-1)3\sigma_g(1)1\pi_{yg}(-1)$	.416
							$3\sigma_g(-1)1\delta g(1)1\pi_{yu}(-1)3\sigma_g(1)1\pi_{xg}(-1)$	.416
39	Σ_g^+	-197.379	52.11	.000	.96[3]	.16[11]	$3\sigma_g(-1)1\delta g(1)1\pi_{xu}(-1)3\sigma_g(1)1\pi_{xg}(-1)$	.504
							$3\sigma_g(-1)1\delta g(1)1\pi_{yu}(-1)3\sigma_g(1)1\pi_{yg}(-1)$	.504
							$3\sigma_g(-1)1\pi_{yg}(-1)1\delta_g(1)3\sigma_u(1)1\pi_{xg}(-1)$	.395
							$3\sigma_g(-1)1\pi_{xg}(-1)1\delta_g(1)3\sigma_u(1)1\pi_{yg}(-1)$	.395
40	Σ_g^+	-197.376	52.17	.000	.84[2]	.47[3]	$7\sigma_g(1)1\pi_{xu}(-2)$	.446
							$7\sigma_g(1)1\pi_{yu}(-2)$	.446
							$3\sigma_g(-1)7\sigma_g(1)1\pi_{xu}(-1)3\sigma_u(1)1\pi_{xg}(-1)$	.327
							$3\sigma_g(-1)7\sigma_g(1)1\pi_{yu}(-1)3\sigma_u(1)1\pi_{yg}(-1)$	.327
41	Σ_g^+	-197.366	52.45	.000	.99[3]	-.04[5]	$3\sigma_g(-1)5\sigma_g(1)1\pi_{xu}(-1)3\sigma_u(1)1\pi_{xg}(-1)$	.537
							$3\sigma_g(-1)5\sigma_g(1)1\pi_{yu}(-1)3\sigma_u(1)1\pi_{yg}(-1)$	.537
42	Σ_g^+	-197.365	52.49	.001	.96[2]	-.28[3]	$1\pi_{xu}(-1)1\pi_{xu}(-1)2\delta_u(1)$	.592
							$3\sigma_g(-1)1\pi_{yu}(-1)2\delta_u(1)3\sigma_u(1)1\pi_{xg}(-1)$	.317
							$3\sigma_g(-1)1\pi_{xu}(-1)2\delta_u(1)3\sigma_u(1)1\pi_{yg}(-1)$	.317
43	Σ_g^+	-197.357	52.68	.001	.73[2]	.68[3]	$3\sigma_g(-1)1\pi_{yu}(-1)2\pi_{yu}(1)$	.427
							$3\sigma_g(-1)1\pi_{xu}(-1)2\pi_{xu}(1)$	.427
44	Σ_g^+	-197.342	53.11	.008	.99[2]	.15[3]	$3\sigma_g(-2)4\sigma_g(1)$	.798
45	Σ_g^+	-197.339	53.19	.002	.73[3]	-.09[10]	$1\pi_{yu}(-2)2\pi_{yu}(1)3\sigma_u(1)1\pi_{yg}(-1)$	.402
							$1\pi_{yu}(-2)2\pi_{xu}(1)3\sigma_u(1)1\pi_{xg}(-1)$	.402
							$3\sigma_g(-1)1\pi_{xu}(-1)2\pi_{yu}(1)$	.370
							$3\sigma_g(-1)1\pi_{yu}(-1)2\pi_{xu}(1)$	.370

[a]Frozen Averaged Natural Orbitals formed from 15 sigma roots. Perturbation selection threshold = 0.6×10^{-5}, as explained in text. CI space = 621289, Ref. space = 84, for ion. Ref. space = 12, CI space = 18604 for neutral molecule. See Table 5 for explanation of columns.
[b]Neutral molecule in this set of FANO.

Table 7. $^2\Pi_u$ states of F_2^+ [a].

	State	Energy	Diff	S_J^2	Dominant orb.		Dominant Configurations	Coeff.
1	Σ_g^+	-199.293					SCF	.947
							$3\sigma_g(-2)3\sigma_g(2)$	.181
1	Π_{xu}	-198.610	18.58	.751	1.00[1]	.01[2]	$1\pi_{xu}(-1)$	.876
							$3\sigma_g(-1)3\sigma_u(1)1\pi_{xg}(-1)$	.342
2	Π_{yu}	-198.393	24.49	.012	.96[1]	.11[2]	$3\sigma_g(-1)3\sigma_u(1)1\pi_{xg}(-1)$	.942
3	Π_{xu}	-198.312	26.70	.000	1.00[1]	.05[2]	$1\pi_{yu}(-1)3\sigma_g(2)1\pi_{yg}(-1)1\pi_{yg}(-1)$	.777
							$1\pi_{xu}(-1)3\sigma_g(2)1\pi_{yg}(-2)$	.513
4	Π_{xu}	-198.213	29.37	.012	1.00[1]	.02[2]	$1\pi_{xu}(-1)3\sigma_g(2)1\pi_{xg}(-2)$	.713
							$1\pi_{yu}(-1)3\sigma_g(2)1\pi_{xg}(-2)$	.447
5	Π_{xu}	-198.144	31.24	.062	1.00[1]	.03[2]	$1\pi_{yu}(-1)3\sigma_g(2)1\pi_{xg}(-1)1\pi_{yg}(-1)$	.330
							$3\sigma_g(-1)3\sigma_u(1)1\pi_{xg}(-1)$	.703
6	Π_{xu}	-198.080	32.99	.004	1.00[1]	.03[2]	$3\sigma_g(-2)1\pi_{xu}(-1)3\sigma_u(2)$	.379
							$1\pi_{xu}(-1)1\pi_{yu}(-2)3\sigma_u(2)$	.632
7	Π_{xu}	-197.935	36.95	.001	.94[1]	-.25[5]	$1\pi_{yu}(-1)3\sigma_g(2)1\pi_{yg}(-1)1\pi_{yg}(-1)$	.592
							$2\pi_{yu}(1)1\pi_{xg}(-1)1\pi_{yg}(-1)$	.811
8	Π_{xu}	-197.907	37.71	.000	.90[1]	.31[5]	$4\sigma_g(1)3\sigma_u(1)1\pi_{xg}(-1)1\pi_{yg}(-2)$	.824
							$4\sigma_g(1)1\pi_{yu}(-2)3\sigma_u(1)1\pi_{xg}(-1)$	.333
9	Π_{xu}	-197.898	37.95	.002	1.00[1]	.04[5]	$2\pi_{xu}(1)1\pi_{yg}(-2)$	.626
							$2\pi_{yu}(1)1\pi_{xg}(-1)1\pi_{yg}(-1)$	.489
10	Π_{xu}	-197.888	38.23	.003	1.00[1]	.06[5]	$2\pi_{xu}(1)1\pi_{yg}(-2)$	.653
							$2\pi_{xu}(1)1\pi_{xg}(-2)$	.349
							$1\pi_{xu}(-2)2\pi_{xu}(1)$	.325
11	Π_{xu}	-197.867	38.78	.000	.99[1]	.10[5]	$4\sigma_g(1)3\sigma_u(1)1\pi_{xg}(-1)1\pi_{yg}(-2)$	.806
							$4\sigma_g(1)1\pi_{yu}(-2)3\sigma_u(1)1\pi_{xg}(-1)$	.352
12	Π_{xu}	-197.777	41.24	.001	.99[1]	-.07[5]	$3\pi_{yu}(1)1\pi_{xg}(-1)1\pi_{xg}(-1)$	.835
13	Π_{xu}	-197.771	41.42	.000	.66[5]	-.19[6]	$1\pi_{yu}(-1)2\pi_{yg}(1)1\pi_{yg}(-1)$	.906

14	Π_{2u}	-197.758	41.76	.000	.96[1]	-.22[5]	$1\pi_{xu}(-1)1\pi_{yg}(-1)2\pi_{yg}(1)$	.606
							$1\pi_{yu}(-1)1\pi_{xg}(-1)2\pi_{yg}(1)$	.595
15	Π_{1u}	-197.754	41.86	.000	.97[1]	.18[5]	$3\pi_{yu}(1)1\pi_{yg}(-1)1\pi_{yg}(-1)$	.758
16	Π_{2u}	-197.736	42.36	.000	.89[1]	-.30[2]	$3\pi_{xu}(1)1\pi_{yg}(-2)$	.565
							$3\pi_{xu}(1)1\pi_{xg}(-2)$	.446
							$1\pi_{yu}(-1)1\pi_{xg}(-1)2\pi_{yg}(1)$	.349
17	Π_{1u}	-197.730	42.52	.000	.99[1]	.07[7]	$1\pi_{xu}(-1)2\sigma_g(-1)3\sigma_u(1)$	.456
							$3\pi_{xu}(1)1\pi_{xg}(-2)$	.415
							$2\sigma_g(-1)3\sigma_u(1)1\pi_{yg}(-1)$	.372
							$1\pi_{xu}(-1)1\pi_{yg}(-1)2\pi_{yg}(1)$	.369
18	Π_{2u}	-197.719	42.81	.000	.91[1]	-.34[5]	$3\sigma_g(-1)4\sigma_u(1)1\pi_{yg}(-1)$	.519
							$3\pi_{xu}(1)1\pi_{xg}(-2)$	.434
19	Π_{2u}	-197.715	42.93	.000	.89[1]	.31[6]	$5\sigma_g(1)3\sigma_u(1)1\pi_{xg}(-1)1\pi_{yg}(-2)$	.793
							$5\sigma_g(1)1\pi_{yu}(-2)3\sigma_u(1)1\pi_{yg}(-1)$	.319
20	Π_{2u}	-197.708	43.11	.000	.97[1]	-.16[5]	$3\sigma_g(-1)4\sigma_u(1)1\pi_{xg}(-1)$	.508
							$1\pi_{xu}(-1)2\sigma_g(-1)3\sigma_u(1)$	.395
							$1\pi_{yu}(-1)1\pi_{yg}(-1)2\pi_{yg}(1)$	.376
21	Π_{2u}	-197.699	43.37	.000	.76[1]	-.60[5]	$3\sigma_g(-1)4\sigma_u(1)1\pi_{yg}(-1)$	.549
							$1\pi_{xu}(-1)1\pi_{xg}(-1)2\pi_{yg}(1)$	.326
							$3\pi_{xu}(1)1\pi_{yg}(-2)$	.321
22	Π_{2u}	-197.694	43.51	.000	.99[1]	.14[6]	$1\delta_g(1)3\sigma_u(1)1\pi_{xg}(-1)1\pi_{yg}(-2)$	.537
							$1\delta_g(1)3\sigma_u(1)1\pi_{yg}(-2)1\pi_{yg}(-1)$	.493
23	Π_{2u}	-197.678	43.93	.001	.99[1]	.14[6]	$1\pi_{yu}(-1)3\sigma_g(1)4\sigma_u(1)1\pi_{xg}(-1)1\pi_{yg}(-1)$	.460
							$1\pi_{xu}(-1)2\sigma_g(-1)3\sigma_u(1)$	.343
							$1\pi_{xu}(-1)3\sigma_g(1)4\sigma_u(1)1\pi_{xg}(-2)$	.323
24	Π_{2u}	-197.671	44.13	.000	.99[1]	.13[6]	$5\sigma_g(1)3\sigma_u(1)1\pi_{xg}(-1)1\pi_{xg}(-2)$	.748
							$5\sigma_g(1)1\pi_{yu}(-2)3\sigma_u(1)1\pi_{yg}(-1)$	.325
25	Π_{2u}	-197.659	44.46	.000	.95[1]	-.22[5]	$3\sigma_g(-1)4\sigma_u(1)1\pi_{yg}(-1)$	.622
							$3\sigma_g(-1)4\sigma_u(1)1\pi_{xg}(-1)$	.441
26	Π_{2u}	-197.645	44.84	.000	.98[1]	.15[6]	$1\pi_{yu}(-1)3\sigma_g(1)4\sigma_u(1)1\pi_{xg}(-1)1\pi_{yg}(-1)$	.502
							$1\delta_g(1)3\sigma_u(1)1\pi_{xg}(-2)1\pi_{yg}(-1)$	.496
							$1\delta_g(1)3\sigma_u(1)1\pi_{yg}(-1)1\pi_{yg}(-2)$	.418
27	Π_{2u}	-197.644	44.85	.000	.99[1]	.10[6]	$1\pi_{yu}(-1)3\sigma_g(1)4\sigma_u(1)1\pi_{xg}(-1)1\pi_{yg}(-1)$	.634
							$1\delta_g(1)3\sigma_u(1)1\pi_{xg}(-1)1\pi_{xg}(-2)$	.356
							$1\delta_g(1)3\sigma_u(1)1\pi_{xg}(-2)1\pi_{yg}(-1)$	.319
28	Π_{2u}	-197.635	45.10	.000	.99[1]	.07[6]	$4\sigma_g(1)1\pi_{xu}(-1)1\pi_{xu}(-1)3\sigma_u(1)1\pi_{xg}(-1)$	.621
							$4\sigma_g(1)1\pi_{yu}(-2)3\sigma_u(1)1\pi_{yg}(-1)$	.329
							$1\pi_{yu}(-1)3\sigma_g(1)4\sigma_u(1)1\pi_{yg}(-1)1\pi_{yg}(-1)$	.303

29	Π_{2u}	-197.624	45.42	.000	1.00[1]	.04[2]	$3\sigma_g(-1)4\sigma_g(1)1\pi_{xu}(-1)$	.587
							$3\sigma_g(-1)4\sigma_u(1)1\pi_{yg}(-1)$	.557
30	Π_{2u}	-197.610	45.80	.000	1.00[1]	.07[6]	$1\pi_{yu}(-1)1\pi_{xg}(-1)2\pi_{yg}(1)$	.476
							$1\pi_{xu}(-1)1\pi_{yg}(-1)2\pi_{yg}(1)$	.459
							$3\sigma_g(-1)3\sigma_u(1)1\pi_{yg}(-1)1\pi_{yg}(-1)2\pi_{yg}(1)$	.336
							$1\pi_{xu}(-1)1\pi_{yu}(-1)2\pi_{yg}(1)$	.322
31	Π_{2u}	-197.597	46.13	.000	1.00[1]	.02[6]	$4\sigma_g(1)1\pi_{xu}(-1)1\pi_{yu}(-1)3\sigma_u(1)1\pi_{yg}(-1)$	.739
32	Π_{2u}	-197.579	46.63	.000	.98[1]	-.12[2]	$4\sigma_g(1)1\pi_{xu}(-1)1\pi_{xu}(-1)3\sigma_u(1)1\pi_{xg}(-1)$	.663
							$4\sigma_g(1)1\pi_{yu}(-2)3\sigma_u(1)1\pi_{xg}(-1)$	.400
33	Π_{2u}	-197.571	46.85	.001	.99[1]	.12[5]	$1\pi_{xu}(-2)2\pi_{xu}(1)$	.396
							$2\pi_{xu}(1)1\pi_{yu}(-2)$	.334
34	Π_{2u}	-197.547	47.49	.001	.98[1]	-.13[2]	$2\sigma_g(-1)3\sigma_u(1)1\pi_{xg}(-1)$	.408
							$3\sigma_g(-1)2\sigma_g(-1)3\sigma_u(2)1\pi_{xg}(-1)$	.321
35	Π_{2u}	-197.500	48.78	.000	.79[1]	-.42[6]	$3\sigma_g(-1)3\sigma_u(1)2\pi_{xg}(1)1\pi_{yg}(-2)$	.806
36	Π_{2u}	-197.479	49.34	.000	.99[1]	.11[6]	$3\sigma_g(-1)1\pi_{xg}(-2)3\sigma_u(1)2\pi_{xg}(1)$	.452
							$1\pi_{xu}(-1)3\sigma_g(1)4\sigma_u(1)1\pi_{xg}(-2)$	.759
							$4\sigma_g(1)1\pi_{xu}(-2)3\sigma_u(1)1\pi_{xg}(-1)$	.301
37	Π_{2u}	-197.469	49.62	.000	1.00[1]	-.02[5]	$3\sigma_g(-1)1\pi_{xu}(-1)2\pi_{xu}(1)3\sigma_u(1)1\pi_{xg}(-1)$	.829

[a]See notes to Table 5. CI space = 852913, Ref. space = 68 for ion. Ref. space = 13, CI space = 18664 for neutral molecule.

Table 8. $^2\Pi_g$ states of F_2^+ [a].

	State	Energy	Diff	S_j^2	Dominant orb.		Dominant Configurations	Coeff.
	$1\Sigma_g^+$	-199.293					SCF	.947
							$3\sigma_g(-2)3\sigma_u(2)$	.181
1	Π_{xg}	-198.729	15.35	.805	1.00[1]	.01[2]	$1\pi_{yg}(-1)$	.909
2	Π_{xg}	-198.394	24.44	.001	1.00[1]	-.01[3]	$3\sigma_u(2)1\pi_{xu}(-1)1\pi_{yg}(-2)$	.859
							$1\pi_{xu}(-2)3\sigma_g(2)1\pi_{yg}(-1)$	.328
3	Π_{xg}	-198.265	27.96	.002	.98[1]	.15[3]	$3\sigma_g(-1)1\pi_{xu}(-1)3\sigma_u(1)$	.936
4	Π_{xg}	-198.155	30.95	.001	1.00[1]	.04[3]	$1\pi_{zu}(-1)1\pi_{yu}(-1)3\sigma_u(2)1\pi_{yg}(-1)$	.883
5	Π_{xg}	-198.116	32.03	.004	1.00[1]	.04[3]	$1\pi_{xu}(-2)3\sigma_g(2)1\pi_{xg}(-1)$	.713
							$1\pi_{xu}(-1)1\pi_{xu}(-1)3\sigma_u(2)1\pi_{yg}(-1)$	.397
6	Π_{xg}	-198.035	34.21	.006	1.00[1]	.07[3]	$1\pi_{xu}(-2)3\sigma_u(2)1\pi_{xg}(-1)$	.366
							$3\sigma_g(-1)1\pi_{xu}(-1)3\sigma_u(1)$	.589
							$1\pi_{xu}(-2)3\sigma_u(2)1\pi_{xg}(-1)$	.443
7	Π_{xg}	-197.868	38.76	.000	.93[1]	-.31[3]	$1\pi_{xu}(-1)1\pi_{xu}(-1)3\sigma_u(2)1\pi_{yg}(-1)$	.375
							$2\pi_{xu}(1)1\pi_{yu}(-1)1\pi_{yg}(-1)$	.315
8	Π_{xg}	-197.865	38.86	.000	.82[1]	-.49[3]	$1\pi_{yu}(-1)2\pi_{yu}(1)1\pi_{xg}(-1)$	.833
							$1\pi_{xu}(-1)2\pi_{yu}(1)1\pi_{yg}(-1)$	.579
							$2\pi_{xu}(1)1\pi_{xu}(-1)1\pi_{xg}(-1)$	.562
9	Π_{xg}	-197.848	39.31	.000	.77[3]	-.43[7]	$1\pi_{xu}(-1)2\pi_{xu}(1)1\pi_{xg}(-1)$	.327
							$1\pi_{yu}(-1)2\pi_{yu}(1)1\pi_{xg}(-1)$	.595
							$1\pi_{xu}(-1)2\pi_{yu}(1)1\pi_{yg}(-1)$	.471
10	Π_{xg}	-197.834	39.70	.000	.90[1]	-.37[3]	$1\pi_{xg}(-1)1\pi_{yg}(-1)2\pi_{xg}(1)$	.462
							$1\pi_{xu}(-1)2\pi_{xu}(1)1\pi_{xg}(-1)$	.647
							$1\pi_{xu}(-1)2\pi_{yu}(1)1\pi_{yg}(-1)$	.357
11	Π_{xg}	-197.825	39.94	.001	1.00[1]	.05[3]	$3\sigma_g(-1)4\sigma_g(1)1\pi_{xg}(-1)$	.316
							$1\pi_{xg}(-1)1\pi_{yg}(-1)2\pi_{yg}(1)$	.710
								.357
12	Π_{xg}	-197.822	40.02	.000	.99[1]	-.14[3]	$1\pi_{xg}(-1)1\pi_{yg}(-1)2\pi_{xg}(1)$	.501
							$3\sigma_g(-1)4\sigma_g(1)1\pi_{xg}(-1)$	.446
13	Π_{xg}	-197.809	40.38	.000	.79[1]	.52[3]	$1\pi_{xu}(-1)2\pi_{xu}(1)1\pi_{xg}(-1)$	.332
							$2\pi_{xg}(1)1\pi_{yg}(-2)$	.662
14	Π_{xg}	-197.807	40.41	.000	.99[1]	-.15[3]	$4\sigma_g(1)1\pi_{yg}(-1)3\sigma_u(1)1\pi_{xg}(-1)1\pi_{xg}(-1)$	.492
							$4\sigma_g(1)1\pi_{xu}(-1)3\sigma_u(1)1\pi_{yg}(-2)$	.472
							$3\sigma_g(1)4\sigma_u(1)1\pi_{xg}(-1)1\pi_{xg}(-2)$	.339
15	Π_{xg}	-197.800	40.62	.000	1.00[1]	-.06[3]	$1\pi_{xg}(-1)1\pi_{xg}(-1)2\pi_{xg}(1)$	.871
							$2\pi_{xg}(1)1\pi_{xg}(-2)$	.351
16	Π_{xg}	-197.791	40.86	.001	1.00[1]	.03[3]	$3\sigma_g(1)4\sigma_u(1)1\pi_{xg}(-1)1\pi_{xg}(-2)$	.650
							$4\sigma_g(1)1\pi_{yu}(-1)3\sigma_u(1)1\pi_{yg}(-1)1\pi_{xg}(-1)$	.365
17	Π_{xg}	-197.781	41.12	.000	1.00[1]	-.08[3]	$4\sigma_g(1)1\pi_{xu}(-1)3\sigma_u(1)1\pi_{xg}(-2)$	.524
							$4\sigma_g(1)1\pi_{yu}(-1)3\sigma_u(1)1\pi_{yg}(-1)$	.471
18	Π_{xg}	-197.779	41.19	.003	1.00[1]	-.03[3]	$1\pi_{xg}(-2)2\pi_{xg}(1)$	.304
							$1\pi_{xg}(-2)2\pi_{yg}(1)$	.577
19	Π_{xg}	-197.760	41.71	.000	.68[1]	-.55[3]	$3\sigma_g(-1)4\sigma_u(1)1\pi_{xg}(-1)$	.609
							$4\sigma_g(1)1\pi_{yu}(-1)3\sigma_u(1)1\pi_{xg}(-1)1\pi_{xg}(-1)$	.569
20	Π_{xg}	-197.756	41.81	.000	1.00[1]	-.06[4]	$4\sigma_g(1)1\pi_{yu}(-1)3\sigma_u(1)1\pi_{xg}(-1)1\pi_{yg}(-1)$	.650
							$3\sigma_g(-1)4\sigma_u(1)1\pi_{xg}(-1)$	.513
21	Π_{xg}	-197.748	42.03	.000	1.00[1]	-.06[4]	$3\sigma_g(1)4\sigma_u(1)1\pi_{xg}(-1)1\pi_{xg}(-2)$	.730
							$4\sigma_g(1)1\pi_{yu}(-1)3\sigma_u(1)1\pi_{xg}(-1)1\pi_{yg}(-1)$	.330
22	Π_{xg}	-197.734	42.41	.001	.99[1]	-.14[3]	$1\pi_{xu}(-1)2\pi_{yu}(1)1\pi_{yg}(-1)$	.541
							$1\pi_{yu}(-1)2\pi_{yu}(1)1\pi_{xg}(-1)$	.503
23	Π_{xg}	-197.670	44.17	.000	.99[1]	-.06[4]	$3\sigma_g(-1)2\pi_{xu}(1)3\sigma_u(1)1\pi_{yg}(-1)1\pi_{yg}(-1)$	.416
							$4\sigma_g(1)1\pi_{xu}(-1)3\sigma_u(1)1\pi_{xg}(-2)$	.769
24	Π_{xg}	-197.669	44.19	.000	1.00[1]	-.04[3]	$3\sigma_g(-1)2\pi_{xu}(1)3\sigma_u(1)1\pi_{yg}(-2)$	.792
							$3\sigma_g(-1)2\pi_{xu}(1)1\pi_{xu}(-2)3\sigma_u(1)$	.446
25	Π_{xg}	-197.659	44.45	.000	1.00[1]	.05[3]	$2\pi_{xu}(1)1\pi_{xu}(-1)1\pi_{yg}(-1)$	.589
							$1\pi_{xu}(-1)2\pi_{xu}(1)1\pi_{yg}(-1)$	.460
26	Π_{xg}	-197.642	44.92	.000	.85[1]	.47[3]	$3\sigma_g(-1)2\pi_{xu}(1)3\sigma_u(1)1\pi_{yg}(-2)$	.344
							$3\sigma_g(-1)2\pi_{xu}(1)3\sigma_u(1)1\pi_{xg}(-2)$	.756
27	Π_{xg}	-197.641	44.94	.001	1.00[1]	.04[3]	$3\sigma_g(-1)1\pi_{xg}(-2)2\pi_{xu}(1)3\sigma_u(1)$	.435
							$1\pi_{yu}(-1)2\pi_{yu}(1)1\pi_{yg}(-1)$	.519
							$1\pi_{xu}(-1)2\pi_{yu}(1)1\pi_{xg}(-1)$	.515
28	Π_{xg}	-197.613	45.72	.000	1.00[1]	-.05[3]	$3\sigma_g(-1)2\pi_{xu}(1)3\sigma_u(1)1\pi_{xg}(-1)1\pi_{xg}(-1)$	.418
							$4\sigma_g(1)1\pi_{xu}(-1)3\sigma_u(1)1\pi_{xg}(-2)$	.758

29	Π_{xg}	-197.598	46.11	.000	.69[1]	-.63[3]	$1\pi_{xg}(-1)3\pi_{yg}(1)1\pi_{zg}(-1)$	.633
							$1\pi_{xg}(-1)3\pi_{yg}(1)1\pi_{yg}(-1)$	.616
30	Π_{xg}	-197.586	46.44	.000	1.00[1]	.04[2]	$4\sigma_g(1)1\pi_{yg}(-1)3\sigma_g(1)1\pi_{xg}(-1)1\pi_{yg}(-1)$	.537
							$4\sigma_g(1)1\pi_{xu}(-1)1\pi_{yu}(-2)3\sigma_u(1)$	.459
31	Π_{xg}	-197.576	46.70	.001	1.00[1]	-.04[3]	$3\sigma_g(-1)4\sigma_g(1)3\sigma_u(2)1\pi_{yg}(-1)1\pi_{yg}(-2)$	.322
							$1\pi_{xu}(-1)2\pi_{zu}(1)1\pi_{zg}(-1)$	.537
							$2\pi_{xu}(1)1\pi_{yu}(-1)1\pi_{zg}(-1)$	.446
							$3\sigma_g(-1)2\pi_{zu}(1)3\sigma_u(1)1\pi_{zg}(-2)$	.342
32	Π_{xg}	-197.565	47.01	.000	1.00[1]	.02[4]	$3\sigma_g(-1)2\pi_{yu}(1)3\sigma_g(1)1\pi_{xg}(-1)1\pi_{yg}(-1)$	.832
							$3\sigma_g(-1)1\pi_{xu}(-1)1\pi_{yu}(-1)2\pi_{yu}(1)3\sigma_u(1)$	.379
33	Π_{xg}	-197.555	47.28	.001	1.00[1]	.06[4]	$3\sigma_g(-1)5\sigma_g(1)1\pi_{xg}(-1)$	.707
							$2\sigma_g(-1)3\sigma_g(1)1\pi_{zg}(-1)$	.301
34	Π_{xg}	-197.519	48.25	.000	.97[1]	-.21[3]	$1\pi_{yu}(-1)1\pi_{yu}(-1)2\pi_{yg}(1)$	.729
							$3\sigma_g(-1)1\pi_{yu}(-1)3\sigma_u(1)1\pi_{zg}(-1)2\pi_{yg}(1)$	.317
							$3\sigma_g(-1)1\pi_{zu}(-1)3\sigma_u(1)1\pi_{yg}(-1)2\pi_{yg}(1)$	.310
35	Π_{xg}	-197.509	48.54	.000	.87[1]	.41[3]	$3\sigma_g(-1)2\pi_{yu}(1)3\sigma_u(1)1\pi_{xg}(-1)1\pi_{yg}(-1)$	.791
							$3\sigma_g(-1)1\pi_{xu}(-1)1\pi_{xu}(-1)2\pi_{yu}(1)3\sigma_u(1)$	.349
36	Π_{xg}	-197.489	49.09	.000	.98[1]	.17[3]	$5\sigma_g(1)1\pi_{yu}(-1)3\sigma_u(1)1\pi_{xg}(-1)1\pi_{yg}(-1)$	.525
							$5\sigma_g(1)1\pi_{xu}(-1)3\sigma_u(1)1\pi_{yg}(-2)$	.492
							$1\pi_{xu}(-1)1\pi_{yu}(-1)3\sigma_g(1)4\sigma_u(1)1\pi_{yg}(-1)$	.457
37	Π_{xg}	-197.482	49.28	.000	.76[1]	-.63[4]	$1\pi_{xu}(-1)1\pi_{yu}(-1)3\sigma_g(1)4\sigma_u(1)1\pi_{xg}(-1)$	.570
							$1\pi_{yu}(-2)3\sigma_u(1)4\sigma_u(1)1\pi_{yg}(-1)$	.391
							$3\sigma_g(-1)1\pi_{xu}(-1)4\sigma_u(1)$	.360
38	Π_{xg}	-197.474	49.48	.000	.97[1]	.21[3]	$5\sigma_g(1)1\pi_{yu}(-1)3\sigma_u(1)1\pi_{xg}(-1)1\pi_{yg}(-1)$	.323
							$3\sigma_g(-1)5\sigma_u(1)1\pi_{zg}(-1)$	.598
							$5\sigma_g(1)1\pi_{zu}(-1)3\sigma_u(1)1\pi_{yg}(-2)$	.405
39	Π_{xg}	-197.471	49.56	.000	.96[1]	.25[3]	$5\sigma_g(1)1\pi_{yu}(-1)3\sigma_u(1)1\pi_{xg}(-1)1\pi_{yg}(-1)$	.378
							$3\sigma_g(-1)5\sigma_u(1)1\pi_{xg}(-1)$	.509
							$5\sigma_g(1)1\pi_{zu}(-1)3\sigma_u(1)1\pi_{yg}(-2)$	.402
40	Π_{xg}	-197.469	49.63	.000	.94[1]	-.30[3]	$5\sigma_g(1)1\pi_{yu}(-1)3\sigma_u(1)1\pi_{xg}(-1)1\pi_{yg}(-1)$	.363
							$3\pi_{xu}(1)1\pi_{yu}(-1)1\pi_{yg}(-1)$	.332
41	Π_{xg}	-197.431	50.66	.000	.98[1]	-.17[3]	$5\sigma_g(1)1\pi_{yu}(-1)3\sigma_u(1)1\pi_{zg}(-1)1\pi_{yg}(-1)$	.691
42	Π_{xg}	-197.429	50.71	.000	.98[1]	-.13[3]	$1\pi_{yu}(-1)4\pi_{yu}(1)1\pi_{zg}(-1)$	.632
							$1\pi_{zu}(-1)4\pi_{yu}(1)1\pi_{yg}(-1)$	.612
43	Π_{xg}	-197.419	50.99	.000	.89[3]	-.12[5]	$3\sigma_g(-1)1\pi_{yu}(-1)3\sigma_u(1)1\pi_{xg}(-1)2\pi_{yg}(1)$	.546
							$3\sigma_g(-1)1\pi_{zu}(-1)3\sigma_u(1)1\pi_{yg}(-1)2\pi_{yg}(1)$	.536

43

44	Π_{xg}	-197.385	51.90	.000	.98[1]	.18[3]	$1\pi_{xu}(-1)1\delta_g(1)3\sigma_u(1)1\pi_{zg}(-1)1\pi_{yg}(-1)$	.858

[a]See notes to Table 5. CI space = 732926, Ref. space = 96 for Ion. Ref. space = 13, CI space = 18684 for neutral molecule.

44

Table 9. $^2\Sigma_u^+$ states of $F_2^{+\,a}$.

	State	Energy	Diff	S_j^2	Dominant orb.		Dominant Configurations	Coeff.
1	Σ_g^+	-199.292					SCF	.947
							$3\sigma_g(-2)3\sigma_u(2)$	.180
1	Σ_u^+	-198.558	19.97	.001	.79[2]	.50[3]	$3\sigma_u(1)1\pi_{yg}(-2)$	.600
							$3\sigma_u(1)1\pi_{xg}(-2)$	.600
2	Σ_u^+	-198.204	29.60	.041	.94[2]	-.35[3]	$3\sigma_g(-2)3\sigma_u(1)$	.521
							$1\pi_{yg}(-2)3\sigma_u(1)$	.444
							$1\pi_{xg}(-2)3\sigma_u(1)$	.444
3	Σ_u^+	-198.095	32.55	.066	.86[2]	-.52[3]	$3\sigma_g(-2)3\sigma_u(1)$	.704
4	Σ_u^+	-198.049	33.83	.003	.83[2]	-.55[3]	$3\sigma_g(-1)1\pi_{yu}(-1)3\sigma_u(2)1\pi_{yg}(-1)$	.644
							$3\sigma_g(-1)1\pi_{xu}(-1)3\sigma_u(2)1\pi_{xg}(-1)$	.644
5	Σ_u^+	-197.946	36.62	.019	1.00[2]	.06[3]	$4\sigma_g(1)1\pi_{yu}(-1)1\pi_{yg}(-1)$	.624
							$4\sigma_g(1)1\pi_{xu}(-1)1\pi_{xg}(-1)$	.624
6	Σ_u^+	-197.900	37.87	.844	1.00[2]	.04[3]	$2\sigma_u(-1)$	.814
7	Σ_u^+	-197.878	38.47	.022	1.00[2]	.04[3]	$4\sigma_u(1)1\pi_{yg}(-2)$	.560
							$4\sigma_u(1)1\pi_{xg}(-2)$	.560
8	Σ_u^+	-197.778	41.24	.001	1.00[2]	.04[3]	$5\sigma_g(1)1\pi_{yu}(-1)1\pi_{yg}(-1)$	.640
							$5\sigma_g(1)1\pi_{xu}(-1)1\pi_{xg}(-1)$	.639
9	Σ_u^+	-197.739	42.26	.000	.98[2]	.22[3]	$3\sigma_g(-1)4\sigma_g(1)3\sigma_u(1)1\pi_{yg}(-2)$	.543
							$3\sigma_g(-1)4\sigma_g(1)3\sigma_u(1)1\pi_{xg}(-2)$	.543
							$3\sigma_g(-1)4\sigma_g(1)1\pi_{xu}(-2)3\sigma_u(1)$	.323
							$3\sigma_g(-1)4\sigma_g(1)1\pi_{yu}(-2)3\sigma_u(1)$	.323
10	Σ_u^+	-197.738	42.27	.001	1.00[2]	.05[3]	$1\pi_{yu}(-1)1\delta_g(1)1\pi_{yg}(-1)$	.456
							$1\pi_{xu}(-1)1\delta_g(1)1\pi_{xg}(-1)$	.456
							$1\delta g(1)1\pi_{xg}(-1)1\pi_{yg}(-1)$	.436
							$1\delta g(1)1\pi_{yg}(-1)1\pi_{xg}(-1)$	.436
11	Σ_u^+	-197.715	42.89	.000	.99[2]	.10[3]	$5\sigma_u(1)1\pi_{yg}(-2)$	.566
							$5\sigma_u(1)1\pi_{xg}(-2)$	.566
12	Σ_u^+	-197.703	43.22	.006	.89[2]	.45[3]	$3\sigma_g(-1)2\pi_{yu}(1)1\pi_{yg}(-1)$	.595
13	Σ_u^+	-197.693	43.51	.000	.91[2]	.41[3]	$3\sigma_g(-1)2\pi_{xu}(1)1\pi_{xg}(-1)$	.595
							$1\pi_{xu}(-1)2\pi_{xu}(1)3\sigma_u(1)1\pi_{yg}(-1)1\pi_{yg}(-1)$	.481
							$2\pi_{xu}(1)1\pi_{xu}(-1)3\sigma_u(1)1\pi_{yg}(-1)1\pi_{yg}(-1)$	.481
							$1\pi_{yu}(-1)2\pi_{yu}(1)3\sigma_u(1)1\pi_{xg}(-2)$	.336
							$1\pi_{yu}(-1)2\pi_{zu}(1)3\sigma_u(1)1\pi_{xg}(-2)$	.336
14	Σ_u^+	-197.667	44.20	.001	.99[2]	-.08[8]	$4\sigma_g(1)1\pi_{yu}(-1)1\pi_{yg}(-1)$	.365
							$4\sigma_g(1)1\pi_{xu}(-1)1\pi_{xg}(-1)$	.365
							$3\sigma_u(1)1\pi_{xu}(-1)2\pi_{xg}(1)1\pi_{yg}(-2)$	.341
							$3\sigma_u(1)1\pi_{xg}(-2)1\pi_{xg}(-1)2\pi_{yg}(1)$	.341
15	Σ_u^+	-197.666	44.23	.001	.97[2]	-.20[3]	$4\sigma_g(1)1\pi_{yu}(-1)1\pi_{yg}(-1)$	.390
							$4\sigma_g(1)1\pi_{xu}(-1)1\pi_{xg}(-1)$	.390
							$3\sigma_u(1)1\pi_{xu}(-1)2\pi_{yg}(1)1\pi_{xg}(-2)$	.312
							$3\sigma_u(1)1\pi_{xg}(-2)1\pi_{xg}(-1)2\pi_{yg}(1)$	.312
16	Σ_u^+	-197.659	44.43	.000	.89[2]	.45[3]	$2\pi_{yu}(1)1\pi_{yu}(-1)3\sigma_u(1)1\pi_{xg}(-1)1\pi_{yg}(-1)$	.380
							$1\pi_{xu}(-1)2\pi_{xu}(1)3\sigma_u(1)1\pi_{yg}(-1)1\pi_{yg}(-1)$	.380
							$3\sigma_u(1)1\pi_{yg}(-1)2\pi_{xg}(1)1\pi_{xg}(-2)$	.350
							$3\sigma_u(1)1\pi_{xg}(-2)1\pi_{xg}(-1)2\pi_{yg}(1)$	.350
17	Σ_u^+	-197.643	44.87	.008	.94[2]	.34[3]	$3\sigma_g(-1)2\pi_{zu}(1)1\pi_{yg}(-1)$	.600
							$3\sigma_g(-1)2\pi_{xu}(1)1\pi_{xg}(-1)$	.600
18	Σ_u^+	-197.593	45.12	.000	.88[2]	-.48[3]	$1\pi_{xu}(-1)2\pi_{yu}(1)3\sigma_u(1)1\pi_{yg}(-1)1\pi_{yg}(-1)$	.474
							$2\pi_{xu}(1)1\pi_{xu}(-1)3\sigma_u(1)1\pi_{yg}(-1)1\pi_{yg}(-1)$	.474
							$1\pi_{yu}(-1)2\pi_{zu}(1)3\sigma_u(1)1\pi_{xg}(-2)$	.365
							$1\pi_{xu}(-1)2\pi_{yu}(1)3\sigma_u(1)1\pi_{xg}(-2)$	.365
19	Σ_u^+	-197.621	45.47	.000	.93[2]	.35[3]	$3\sigma_u(1)1\pi_{yg}(-2)1\pi_{yg}(-1)2\pi_{xg}(1)$	.529
							$3\sigma_u(1)1\pi_{yg}(-1)2\pi_{xg}(1)1\pi_{yg}(-2)$	.529
20	Σ_u^+	-197.587	46.39	.000	1.00[2]	-.02[8]	$7\sigma_g(1)1\pi_{yu}(-1)1\pi_{yg}(-1)$	.641
							$7\sigma_g(1)1\pi_{xu}(-1)1\pi_{xg}(-1)$	.641
21	Σ_u^+	-197.578	46.63	.000	.95[2]	-.26[3]	$3\sigma_g(-1)1\pi_{yu}(-1)3\sigma_u(2)1\pi_{yg}(-1)$	.386
							$3\sigma_g(-1)1\pi_{xu}(-1)3\sigma_u(2)1\pi_{xg}(-1)$	.386
							$1\pi_{yu}(-1)2\pi_{yu}(1)3\sigma_u(1)1\pi_{yg}(-2)$	.311
							$1\pi_{yu}(-1)2\pi_{yu}(1)3\sigma_u(1)1\pi_{zg}(-2)$	.311
22	Σ_u^+	-197.549	47.43	.000	.86[3]	-.04[4]	$1\pi_{yu}(-1)2\pi_{yu}(1)3\sigma_u(1)1\pi_{zg}(-2)$	.438
							$1\pi_{xu}(-1)2\pi_{xu}(1)3\sigma_u(1)1\pi_{yg}(-2)$	.438
23	Σ_u^+	-197.507	48.57	.000	.96[2]	.29[3]	$1\pi_{yu}(-1)2\pi_{xu}(1)3\sigma_u(1)1\pi_{xg}(-2)$	.523
							$1\pi_{xu}(-1)2\pi_{yu}(1)3\sigma_u(1)1\pi_{yg}(-2)$	.523
24	Σ_u^+	-197.495	48.88	.000	.92[2]	-.34[3]	$1\pi_{yu}(-2)4\sigma_u(1)$	.454
							$1\pi_{xg}(-2)4\sigma_u(1)$	.454
							$3\sigma_g(-1)1\pi_{xu}(-1)3\sigma_u(1)4\sigma_u(1)1\pi_{yg}(-1)$	.320
							$3\sigma_g(-1)1\pi_{yu}(-1)3\sigma_u(1)4\sigma_u(1)1\pi_{xg}(-1)$	.320

25	Σ_u^+	-197.477	49.38	.001	1.00[2]	.03[3]	$1\pi_{xu}(-1)1\delta_g(1)1\pi_{yg}(-1)$	.580
							$1\pi_{yu}(-1)1\delta_g(1)1\pi_{xg}(-1)$	.580
							$3\sigma_g(-1)1\delta_g(1)3\sigma_u(1)1\pi_{xg}(-1)1\pi_{yg}(-1)$	.386
26	Σ_u^+	-197.465	49.72	.000	1.00[2]	.08[3]	$2\sigma_u(-1)3\sigma_u(2)1\pi_{xg}(-2)$	.317
							$2\sigma_u(-1)3\sigma_u(2)1\pi_{yg}(-2)$	.317
27	Σ_u^+	-197.454	50.02	.000	.76[2]	-.65[3]	$6\sigma_u(1)1\pi_{xg}(-2)$	.542
							$6\sigma_u(1)1\pi_{yg}(-2)$	.542
28	Σ_u^+	-197.444	50.28	.000	.75[3]	-.09[8]	$3\sigma_g(-1)1\pi_{xu}(-1)3\sigma_u(1)4\sigma_u(1)1\pi_{xg}(-1)$	.641
							$3\sigma_g(-1)1\pi_{yu}(-1)3\sigma_u(1)4\sigma_u(1)1\pi_{yg}(-1)$	.641

[a]See notes for Table 5. CI space = 725569, Ref. space = 74 for ion. Ref. space = 13, CI space = 18907 for neutral molecule.

Figure Captions

Figure 1. Valence shell binding energy spectra of F_2 from 14 eV to 60 eV at a total energy of 1500 eV. (a) For $\phi = 10°$, (b) for $\phi = 0°$, (c) for $\phi = 0° + 10°$. Vertical ionization potentials of the $1\pi_g$, $1\pi_u$, $3\sigma_g$, $2\sigma_u$, and $2\sigma_g$ orbitals of F_2 are marked along the top (a) respectively. Fitting of the experimental data is indicated by the solid lines, with the dashed lines representing individual Gaussians corresponding to the various valence orbitals. The energy positions and Franck-Condon widths are taken from PES studies [39, 57]. The Gaussian widths are a combination of the instrumental width of the EMS spectrometer and the respective Franck-Condon widths.

Figure 2. Measured and calculated binding energy spectra of F_2 from 14 eV to 60 eV. (a) Measured EMS spectrum at $\phi = 0° + 10°$. The solid curve through the points is the sum of Gaussian functions fitted to the experimental spectrum using the PES energy position, and the convoluted width of the EMS instrumental width and the PES width [39, 57]. (b) using Green's function ADC(4) calculation with [5s4p1d] basis set (Braunschweig). (c) Direct-CI calculation using the Dunning's [5s3p1d] basis set (Perugia). (d) Multireference singles and doubles CI calculation, 199-G(CI) (Indiana). In the calculated binding energy spectra of figure (b)-(d) the theoretical pole energies and pole strengths from the three many-body calculations were used. The angular dependence is determined from the 199-G(MR-CI) wavefunction (see Figs. 3-7). The same energy peak widths as used in figure 2(a) have been folded into the synthesized spectra. See text for details.

Figure 3. Spherically averaged experimental and theoretical momentum profiles for the $1\pi_g$ orbital of molecular fluorine. The solid circles and squares are the experiments A and B respectively. All theoretical momentum distributions have been folded with the experimental momentum resolution using the GW-PG method [31]. See text and Table 1 for further details of the experiment, theoretical methods, basis sets and normalization procedures. The lower panels show the momentum and position space density maps for an oriented F_2 molecule calculated using the 6-311+G* Hartree-Fock wavefunction (see Table 1). The contours are 0.01, 0.02, 0.05, 0.1, 0.2, 0.5, 1.0, 2.0, 5.0, 10.0, 20.0, 50.0, and 90% of the maximum density. The side panels of the density maps (right and top) show the density slices along the axes (dashed vertical and horizontal lines) for each density map.

Figure 4. Spherically averaged experimental and theoretical momentum profiles for the $1\pi_u$ orbital of molecular fluorine. The solid circles and squares are the experiments A and B respectively. All theoretical momentum distributions have been folded with the experimental

momentum resolution using the GW-PG method [31]. See text and Table 1 for further details of the experiment, theoretical methods, basis sets and normalization procedures. The lower panels show the momentum and position space density maps for an oriented F_2 molecule calculated using the 6-311+G* Hartree-Fock wavefunction (see Table 1). The contours are 0.01, 0.02, 0.05, 0.1, 0.2, 0.5, 1.0, 2.0, 5.0, 10.0, 20.0, 50.0, and 90% of the maximum density. The side panels of the density maps (right and top) show the density slices along the axes (dashed vertical and horizontal lines) for each density map.

Figure 5. Spherically averaged experimental and theoretical momentum profiles for the $3\sigma_g$ orbital of molecular fluorine. The solid circles and squares are the experiments A and B respectively. All theoretical momentum distributions have been folded with the experimental momentum resolution using the GW-PG method [31]. See text and Table 1 for further details of the experiment, theoretical methods, basis sets and normalization procedures. The lower panels show the momentum and position space density maps for an oriented F_2 molecule calculated using the 6-311+G* Hartree-Fock wavefunction (see Table 1). The contours are 0.01, 0.02, 0.05, 0.1, 0.2, 0.5, 1.0, 2.0, 5.0, 10.0, 20.0, 50.0, and 90% of the maximum density. The side panels of the density maps (right and top) show the density slices along the axes (dashed vertical and horizontal lines) for each density map.

Figure 6. Spherically averaged experimental and theoretical momentum profiles for the $2\sigma_u$ orbital of molecular fluorine. The experimental data were obtained by deconvoluting the peak at 37.5 eV, plus the contribution from the intensity in the energy range of 25-35 eV of the binding energy spectra (see Fig. 1). All theoretical momentum distributions have been folded with the experimental momentum resolution using the GW-PG method [31]. See text and Table 1 for further details of the experiment, theoretical methods, basis sets and normalization procedures. The dashed line is the 199-G(MR-CI) calculation for the peak at 37.87 eV (Table 4) multiplied by a factor of 0.8. The lower panels show the momentum and position space density maps for an oriented F_2 molecule calculated using the 6-311+G* Hartree-Fock wavefunction (see Table 1). The contours are 0.01, 0.02, 0.05, 0.1, 0.2, 0.5, 1.0, 2.0, 5.0, 10.0, 20.0, 50.0, and 90% of the maximum density. The side panels of the density maps (right and top) show the density slices along the axes (dashed vertical and horizontal lines) for each density map.

Figure 7. Spherically averaged experimental and theoretical momentum profiles for the $2\sigma_g$ orbital of molecular fluorine. The solid dots are the experimental data corresponding to the main peak at 42.1 eV (see Fig. 1). All theoretical momentum distributions have been folded

with the experimental momentum resolution using the GW-PG method [31]. See text and Table 1 for further details of the experiment, theoretical methods, basis sets and normalization procedures. The dashed line is the 199-G(MR-CI) calculation (for the main $2\sigma_u$ pole at 42.91 - see Tables 4 and 6) scaled by a factor of 0.6. The lower panels show the momentum and position space density maps for an oriented F_2 molecule calculated using the 6-311+G* Hartree-Fock wavefunction (see Table 1). The contours are 0.01, 0.02, 0.05, 0.1, 0.2, 0.5, 1.0, 2.0, 5.0, 10.0, 20.0, 50.0, and 90% of the maximum density. The side panels of the density maps (right and top) show the density slices along the axes (dashed vertical and horizontal lines) for each density map.

Figure 8. Spherically averaged experimental and theoretical momentum profiles for the $2\sigma_g$ orbital of molecular fluorine. (a) The experimental data were obtained by summing the intensity over the energy range from 38-60 eV of the binding energy spectra at each ϕ angle. All theoretical momentum distributions have been folded with the experimental momentum resolution using the GW-PG method [31]. See text and Table 1 for further details of the experiment, theoretical methods, basis sets and normalization procedures. The dashed line is the 199-G(MR-CI) calculation scaled by a factor of 0.75. (b) The experimental momentum profile summed over the energy range of 47-57 eV compared with the 199-G(MR-CI) calculation scaled by a spectroscopic factor of 0.13.

Figure 9. Experimental momentum profiles for the outer valence σ_g orbitals of F_2 (this work), Cl_2 [20], Br_2 [21] and I_2 [32]. The solid lines are fits to the data points.

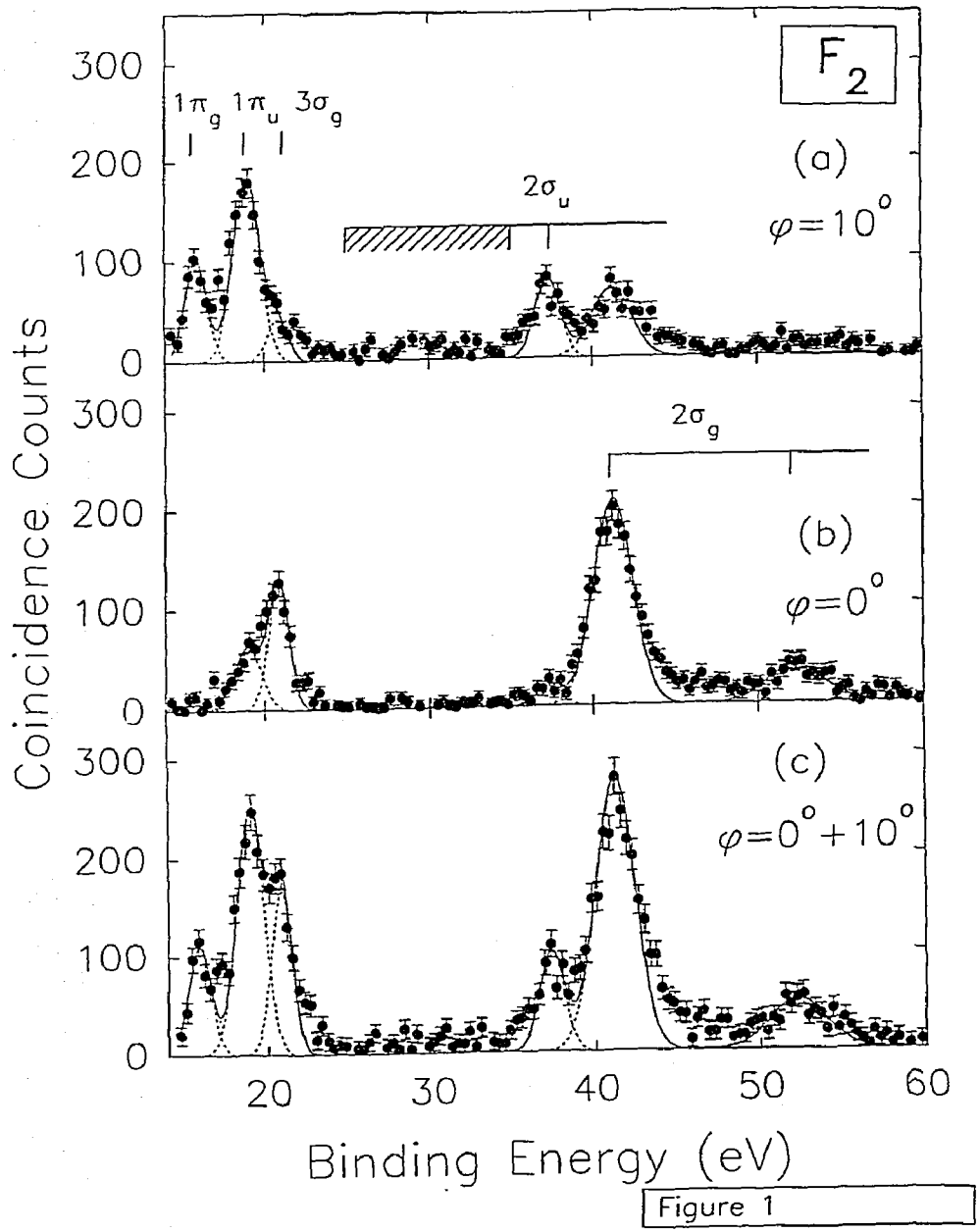

Figure 1

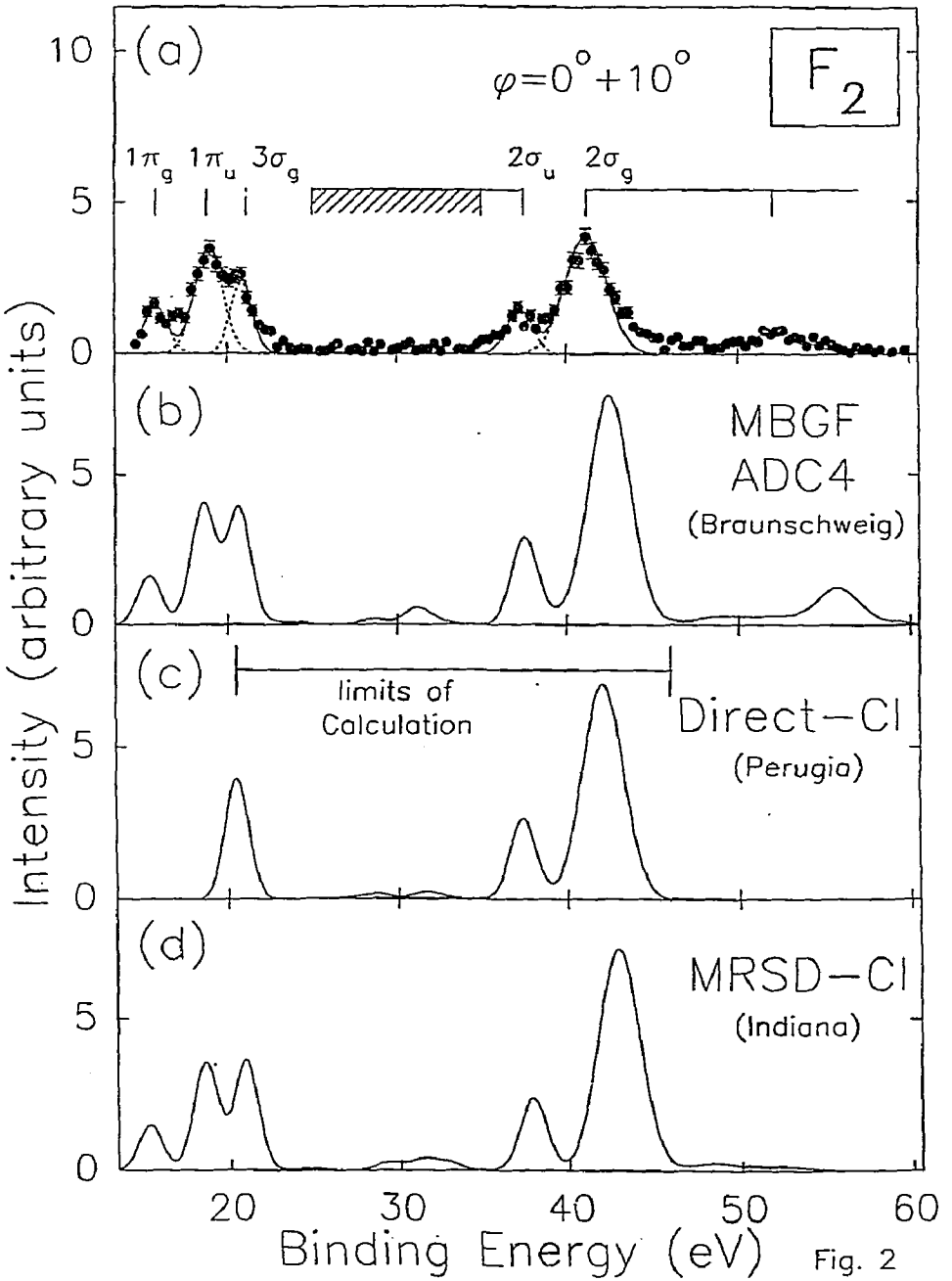

Fig. 2

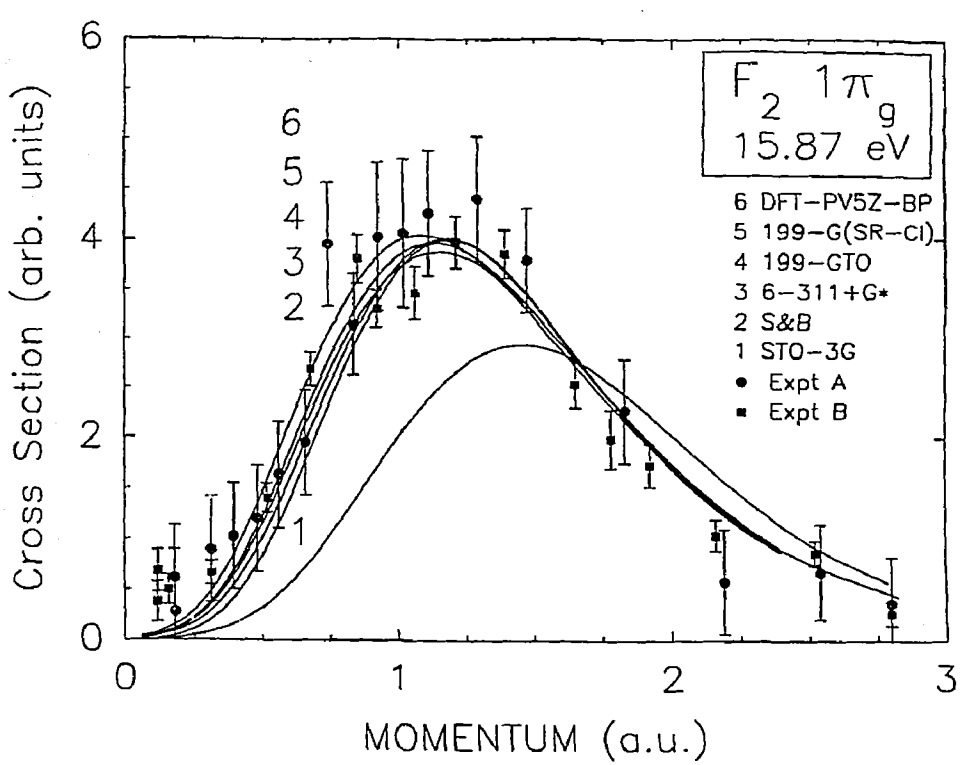

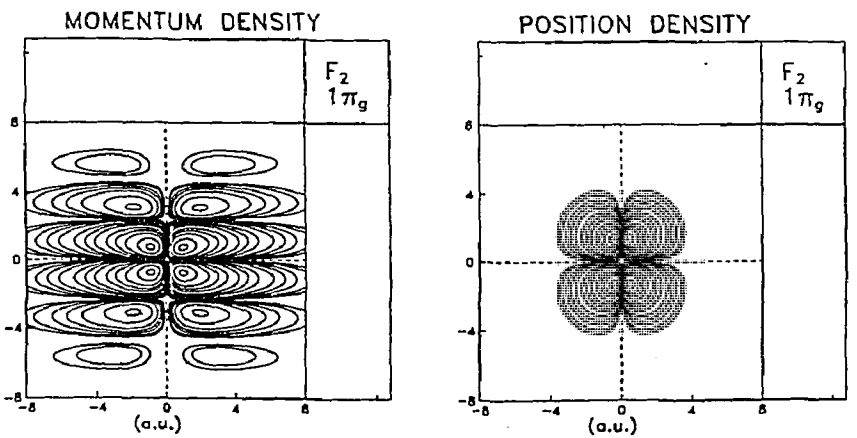

Figure 3

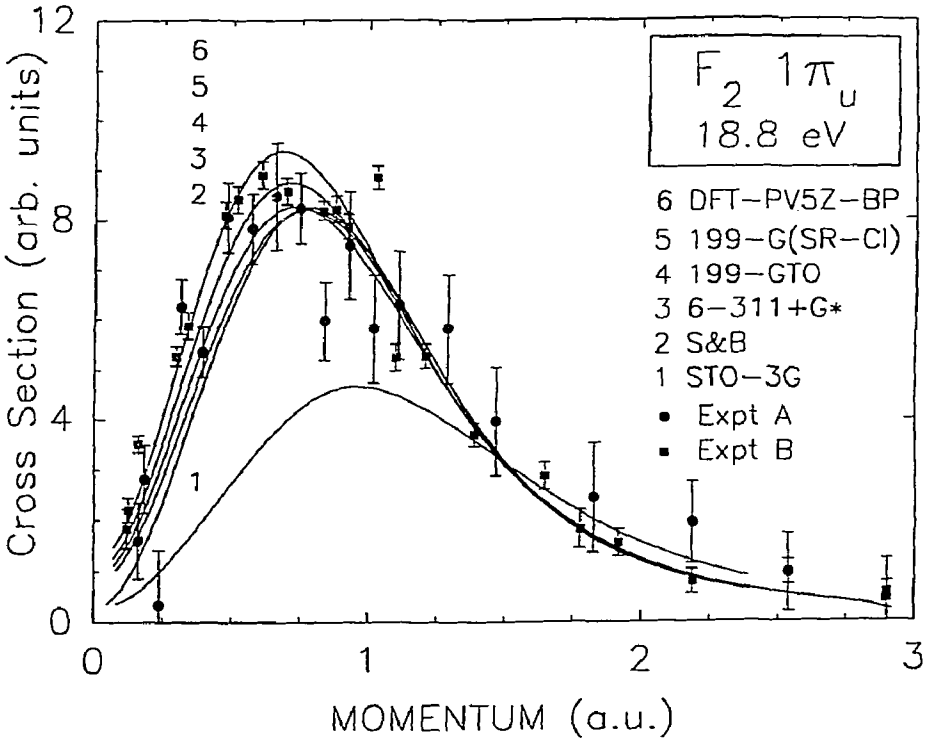

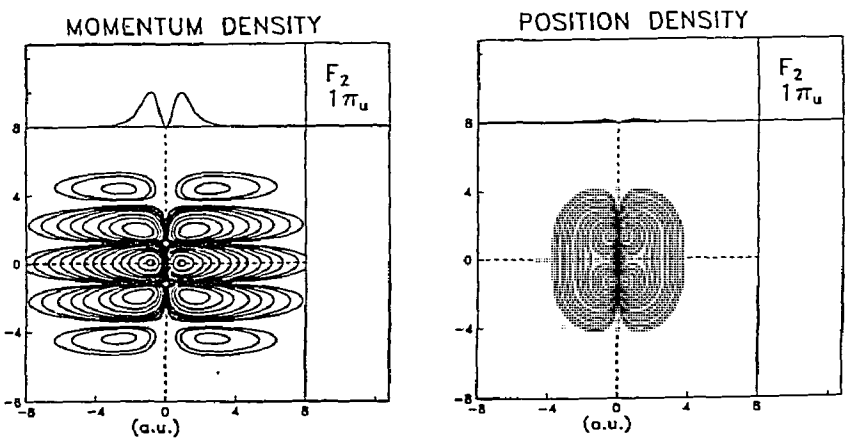

Figure 4

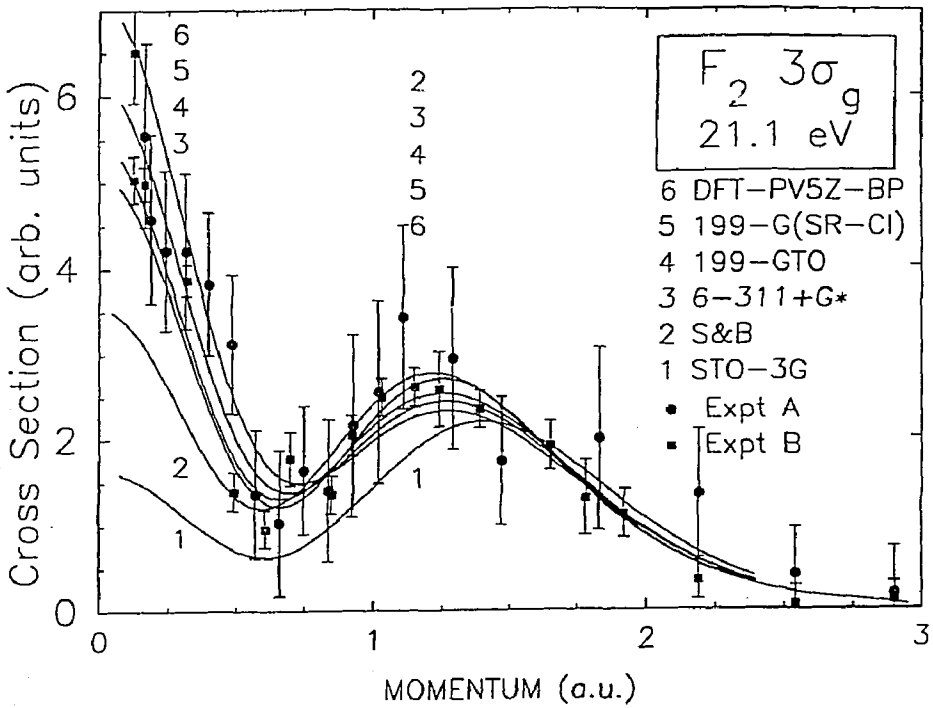

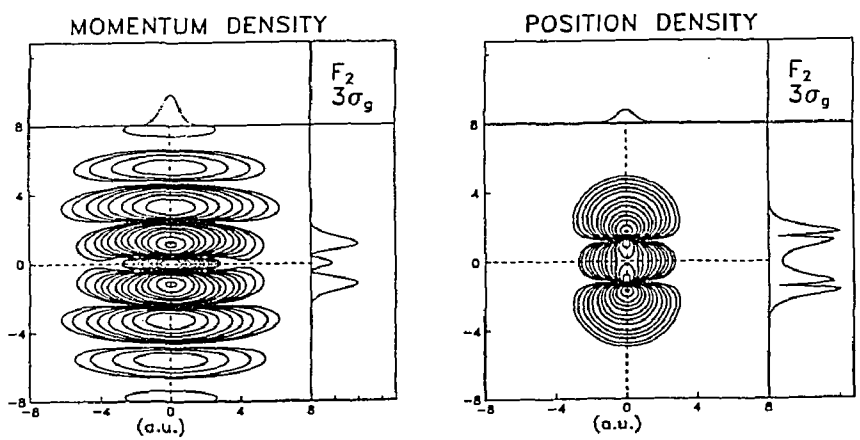

Figure 5

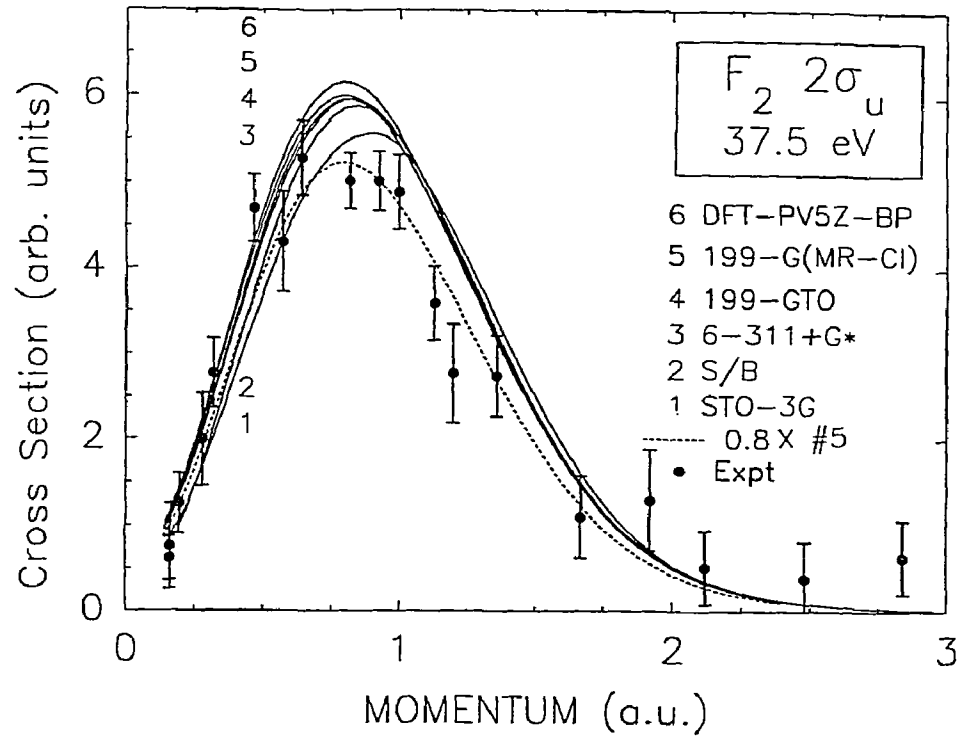

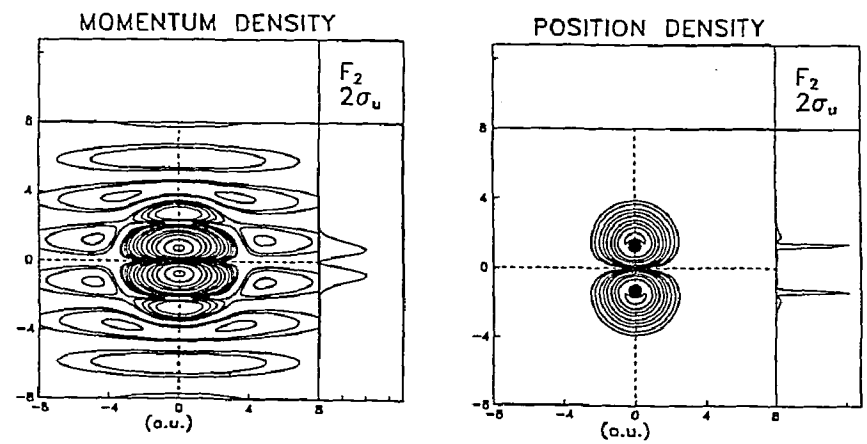

Figure 6

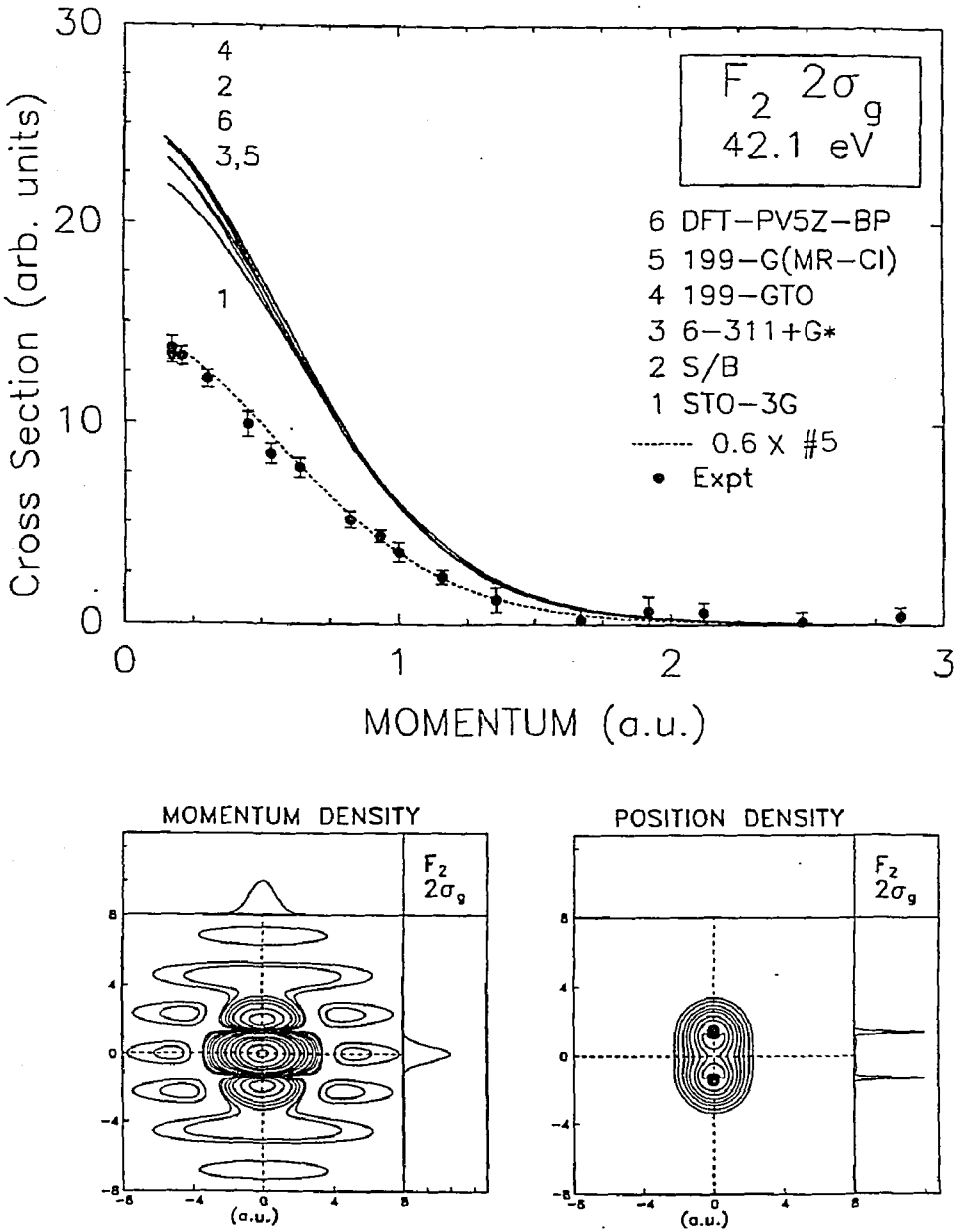

Figure 7

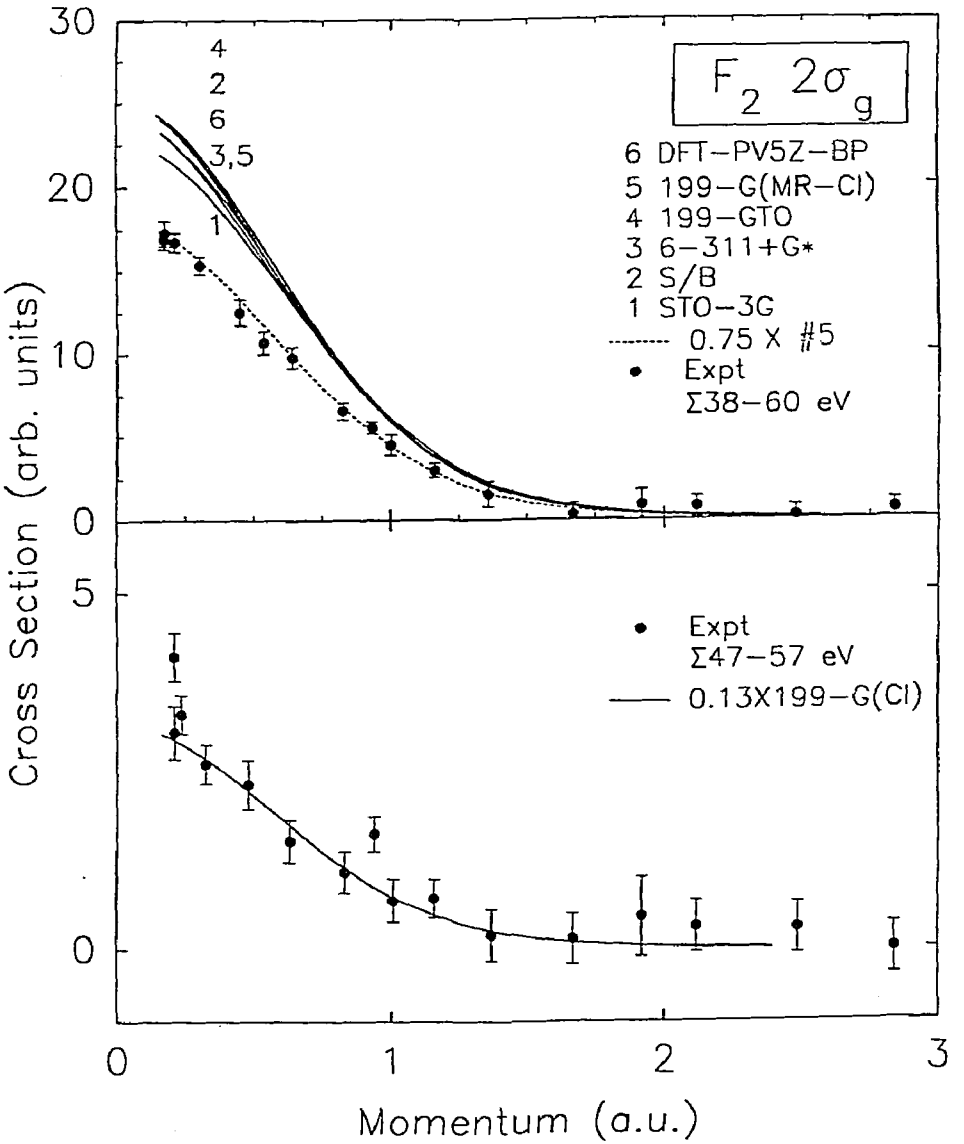

Figure 8

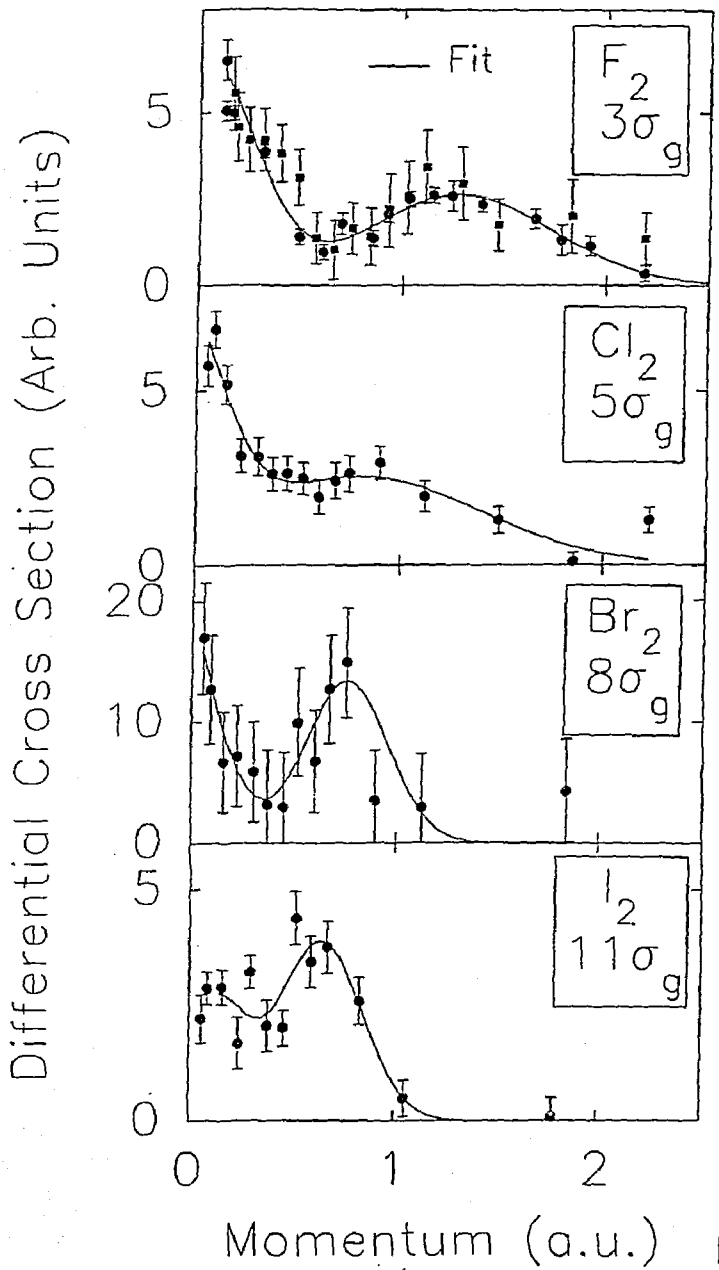
Differential Cross Section (Arb. Units)
Fit
F_2 $3\sigma_g$
Cl_2 $5\sigma_g$
Br_2 $8\sigma_g$
I_2 $11\sigma_g$
5
0
5
0
20
10
0
5
0
0
1
2
Momentum (a.u.)

Figure 9